Title

Real-time physiological measurements of oxygen using a non-invasive self-referencing optical fiber microsensor

Journal

Nature Protocols, 15(2)

ISSN

1754-2189

Authors

Ferreira, Fernando
Luxardi, Guillaume
Reid, Brian
et al.

Publication Date

2020-02-01

DOI

10.1038/s41596-019-0231-x

Peer reviewed

nature protocols

PROTOCOL

https://doi.org/10.1038/s41596-019-0231-x

Real-time physiological measurements of oxygen using a non-invasive self-referencing optical fiber microsensor

Fernando Ferreira[1,2*], Guillaume Luxardi[1], Brian Reid[1], Li Ma[1,3], VijayKrishna Raghunathan[4,5,6] and Min Zhao[1,7*]

Reactive molecular oxygen (O_2) plays important roles in bioenergetics and metabolism and is implicated in biochemical pathways underlying angiogenesis, fertilization, wound healing and regeneration. Here we describe how to use the scanning micro-optrode technique (SMOT) to measure extracellular fluxes of dissolved O_2. The self-referencing O_2-specific micro-optrode (also termed micro-optode and optical fiber microsensor) is a tapered optical fiber with an O_2-sensitive fluorophore coated onto the tip. The O_2 concentration is quantified by fluorescence quenching of the fluorophore emission upon excitation with blue–green light. The micro-optrode presents high spatial and temporal resolutions with improved signal-to-noise ratio (in the picomole range). In this protocol, we provide step-by-step instructions for micro-optrode calibration, validation, example applications and data analysis. We describe how to use the technique for cells (*Xenopus* oocyte), tissues (*Xenopus* epithelium and rat cornea), organs (*Xenopus* gills and mouse skin) and appendages (*Xenopus* tail), and provide recommendations on how to adapt the approach to different model systems. The basic, user-friendly system presented here can be readily installed to reliably and accurately measure physiological O_2 fluxes in a wide spectrum of biological models and physiological responses. The full protocol can be performed in ~4 h.

Introduction

Organisms have adapted to the reactive oxic environment, and most known life forms currently depend on diatomic or molecular oxygen, or dioxygen (O_2), in particular for bioenergetics and metabolism[1,2]. O_2 is a powerful oxidant and, once life forms adapted to use O_2 as the final electron acceptor in oxidative phosphorylation (cellular aerobic respiration), energy output markedly increased[3]. This gave life forms degrees of freedom that permitted unprecedented and massive complexification, diversification and radiation of species[4,5]. In addition, O_2 has a role in cell signaling and behavior, whether related to bioenergetics or not[6,7]. O_2 plays a key role in tracheal branching and lung development[8,9], vasculogenesis and angiogenesis[10], placentation[11], brain development[12], maintenance of pluripotency in stem cell niches[13], and tumors[14,15]. Furthermore, O_2 is important to cell migration, proliferation and differentiation[11,16,17], wound healing[18–20], and regeneration[21–24]. Many of these functions are not controlled directly or strictly by molecular oxygen, but by master players of O_2 homeostasis and physiology: reactive oxygen species (ROS) and hypoxia-inducible factors (HIFs). ROS are the products of the serial oxidation of O_2 to water (H_2O) in a four-electron gain. Most ROS are unstable and extremely reactive, perpetuating chain reactions that are noxious for cells[25,26]. Therefore, enzymatic and non-enzymatic antioxidant strategies evolved and are now ubiquitous in most life forms. The pro-oxidant/antioxidant balance in cells and in the extracellular milieu is indeed crucial for both the signaling and destructive powers of ROS[25]. As life forms grew dependent on O_2, sensing its deprivation (so-called hypoxia) became essential to allow immediate actions for cellular or organismal survival. HIFs are not only O_2 sensors but also transcription factors, regulating

[1]Department of Dermatology, Institute for Regenerative Cures, University of California, Davis, Davis, CA, USA. [2]Centro de Biologia Molecular e Ambiental (CBMA), Departamento de Biologia, Universidade do Minho, Braga, Portugal. [3]Skin and Cosmetic Research Department, Shanghai Skin Disease Hospital, Shanghai, China. [4]Department of Basic Sciences, College of Optometry, University of Houston, Houston, TX, USA. [5]The Ocular Surface Institute, College of Optometry, University of Houston, Houston, TX, USA. [6]Department of Biomedical Engineering, Cullen College of Engineering, University of Houston, Houston, TX, USA. [7]Department of Ophthalmology, Institute for Regenerative Cures, University of California, Davis, Sacramento, CA, USA. *e-mail: id3955@alunos.uminho.pt; minzhao@ucdavis.edu

the expression of hundreds of genes related to bioenergetics and other processes and functions[27]. This brief overview demonstrates that studying O_2 dynamics is of pivotal significance across biological sciences. Therefore, technologies and methods to reliably and accurately quantify O_2 (ref. [28]) are indispensable research tools for investigators.

In a recent study, we demonstrated the integrated role that the three core players of molecular oxygen homeostasis—O_2 itself, ROS and HIFs—play in *Xenopus laevis* tail regeneration. Using an optics-based probe (optrode), we were able to directly measure an O_2 influx following tail amputation. We showed that the O_2 influx correlates with the regeneration of the tadpole tails and is dependent on both ROS production and HIF-1α stabilization[24]. The O_2 concentration was quantified by fluorescence quenching of the O_2-sensitive fluorophore located at the tip of the optrode.

There is an increasing interest in optics-based measurements as a mainstream tool to quantify molecular oxygen flux, and the validated protocol herein is intended not only to offer a basic, user-friendly solution to reliably measure physiologically meaningful O_2 fluxes, but also to stimulate investigators in the exploration of the redox phenomena in biology.

Overview of the procedure

In this protocol, we describe the step-by-step procedures for quantifying O_2 using SMOT and provide example applications and data from various model organisms. We measure O_2 fluxes in *X. laevis* oocytes, epithelium, gills and tails, rat cornea and mouse skin. The procedure consists of five key stages: in the first two stages, we describe how to calibrate (Steps 1–6) and validate (Steps 7–13) the optrode; in the third stage (Step 14), we discuss how to set up data acquisition; in the fourth stage (Steps 15–27), we provide instructions for obtaining detailed experimental measurements; and in the fifth stage (Steps 28 and 29), we delineate strategies for data analysis.

Development of the fluorescence quenching–based method

The seed of the optrode-based method described in this protocol was the mathematical formulation for fluorescence quenching by Stern and Volmer in 1919 (ref. [29]; Box 1). Because O_2 has been shown to be one of the best fluorescence quenchers[30,31], its measurement using optics-based sensors was a natural alternative, as well as a step forward, further elicited to address the polarographic electrode pitfalls. The seminal studies for optical sensing of O_2 occurred in the 1930s, when a fluorometer detected trace amounts of O_2 from a gaseous sample flowing through fluorophore-coated silica particles[30,32,33]. Developments in the 1960 and 1970s led to the inclusion of optical fibers, marking the emergence and the coining of optrodes (linguistic analogy with electrodes) or optodes (from the Greek for 'optical way')[32,34,35]. Some 30 years after Clark's polarographic electrode milestone, a functionally equivalent optrode was used to similarly measure mammalian blood partial pressure of oxygen (pO_2)[36]. O_2 was initially quantified as a function of fluorescence amplitude (intensity), with the introduction of concurrent quantification via fluorescence decay time (lifetime) in 1988 (ref. [37]; Box 1). The sensor developments culminated in staple micro-optrodes in the l990s, tested and used mainly in aquatic microbial biology[38–42].

The next advance was the incorporation of self-referencing capabilities within the optrode system in the mid-2000s[43]. Technological advancements in optical fibers, light sources (including light-emitting diodes (LEDs)), photodiodes, cameras, motion control and software decreased the cost and improved the sensor system, progressing it to the modern, herein-described, state[44]. These developments broadened the use of optrodes to measure O_2 fluxes, with an emphasis on plant physiology, for which various research and technical essays appeared[28,43,45–49]. Our research studies, however, focus on animal physiology and are carried out using SMOT to measure the extracellular fluxes of dissolved O_2 (Fig. 1a). The self-referencing O_2-specific micro-optrode quantifies the analyte concentration by quenching of the fluorescence emitted by an O_2-sensitive fluorophore excited with blue–green light ($\lambda = 505$ nm; Fig. 1b,c)[31].

Comparison with other approaches to quantify physiological O_2

A wealth of established and emerging alternative technologies and methods are being used to measure or image O_2 dynamics[28,32]. Approaches based on redox (e.g., Clark electrode), optical (e.g., optrodes, planar sensor foils and sensor cartridges in a plate reader (Agilent's Seahorse)), molecular (e.g., molecular probes (Luxcel Biosciences' MitoImage), nanosensor and quantum dot, and microscopy (e.g., electron paramagnetic resonance and fluorescence resonance energy transfer)

Box 1 | Fundamentals of fluorescence lifetime–based oxygen measurement

The SMOT system quantifies oxygen (in liquid or gas phase measurement) via fluorescence quenching, with high spatial and temporal resolutions (Table 1). By definition, fluorescence quenching is a process in which the fluorescence intensity of a sample diminishes. Numerous physicochemical interactions can produce quenching; among them is the collisional (or dynamic) quenching by which the O_2 analyte is quantified. In this interaction, a fluorophore (fluorescence emitter) and a quencher collide, during the lifetime of the excited state, leading to energy transfer from the former to the latter that quenches the fluorescence intensity[28,31,32]. O_2 is a well-known and common collisional quencher that can be quantified by many fluorophores[30,31]. We use ready-to-use micro-optrodes that rely on the proprietary fluorophore PSt1 (commercially available from PreSens), which is a proprietary transition metal complex coated as a solid-state matrix onto the optical fiber tapered tip. PSt1 is excited by blue-green light ($\lambda = 505$ nm) from an LED source. In the absence of O_2, the sensor emits fluorescence; in the presence of O_2, there is instead, energy transfer by collision that quenches the fluorescence emission and energizes O_2 from the ground (triplet) to the excited (singlet) state, without consuming it (Fig. 1c). The quenching degree is directly proportional to the O_2 content, providing a reliable measurement.

Both fluorescence amplitude (intensity) and decay time (lifetime) decrease in the presence of O_2. The relationship between oxygen concentration, and fluorescence intensity and lifetime is described by the Stern–Volmer equation[29,31]:

$$\frac{F_0}{F} = \frac{\tau_0}{\tau} = 1 + K_{SV} \times [O_2], \quad (1)$$

where F_0 and F are the fluorescence intensity in the absence and presence of O_2, respectively; τ_0 and τ are the fluorescence decay in the absence and presence of O_2, respectively; K_{SV} is the Stern–Volmer constant and $[O_2]$ is the O_2 (quencher) concentration.
The interface software ASET (Box 3) calculates O_2 concentration using the fluorescence lifetime–based method (phase-modulation or frequency-domain), instead of the fluorescence intensity–based method. For accurate measurements, the fluorescence intensity–based method increases the excitation energy (i.e., laser/light intensity); however, this enhanced sensitivity leads to a substantial increase in fluorophore photobleaching and, consequently, shorter sensor longevity. The sensitivity–photobleaching–longevity tradeoff, in addition to frequent calibration because of noise and drift in excitation sources, shifted the design of the current system in favor of the frequency-domain lifetime–based method[28,32,37,45,76]. This method relies on the O_2-dependent phase angle shift. Phase angle is a measure of the time delay in the emitted fluorescence caused by the decay of the fluorophore when excited by a frequency-modulated light (sine wave; Fig. 2b). The relationship between phase angle and decay time is described by the following equation[45]:

$$\tan\varphi = 2\pi \times f_{mod} \times \tau, \quad (2)$$

where φ is the phase angle and f_{mod} is the modulation frequency.
Finally, O_2 concentration is derived using a modified Stern–Volmer equation:

$$\frac{\tan\varphi_0}{\tan\varphi} = \frac{\tau_0}{\tau} = 1 + K_{SV} \times [O_2]. \quad (3)$$

The relationship between the phase angle and O_2 concentration is nonlinear for the pO_2 0–100% full range and is inversely proportional[28,31,77]. However, for the pO_2 0–32% range, the relationship is almost perfectly linear (generally $r^2 > 0.999$). This range encompasses the physiologically meaningful O_2 tensions; consequently, a two-point calibration (sulfite- or N_2 (gas)–purged and O_2-saturated water) suffices to calibrate the micro-optrode[45,47,49].
In specific terms, the ASET software communicates with the electronic firmware, which has an embedded microprocessor that automatically and in real-time calculates pO_2 (%). The calculation follows the above-detailed fluorescence lifetime–based method via the Stern–Volmer equation based on a measurement of phase angle shift relative to calibration values obtained (at known temperature and barometric pressure) for the sensor being used. The ASET software provides extractable raw data for the oxygen content as percentages (Box 4).

measurements and imaging yield different outcomes in the qualitative-to-quantitative spectrum[28,32,47,50–55].

The approach described in this protocol allows for quantitative determination of extracellular O_2 fluxes using a non-invasive self-referencing micro-optrode. The key alternative approach to this is the classic Clark-type (polarographic) microelectrode[51,56]. Polarographic microelectrodes are electrochemical-based sensors that were used for the majority of the seminal and classic studies of O_2 homeostasis and physiology, including respirometry[28,56,57]. The first of these electrodes was developed in 1953 to measure the pO_2 in blood and has since been improved and adapted into various forms[52,58]. Polarographic electrodes are based on redox reactions consuming the analyte. The probe is polarized to reduce O_2, quantifying O_2 concentration as a function of the generated current (linear relationship). Local (sensor-tip microenvironment) electric field generation and/or disturbance (due to the polarized electrode) and chemical disturbance (due to analyte consumption) are substantial disadvantages, especially for large sensors, which require stirring of the aqueous medium at constant speed to maintain diffusion equilibrium. In addition, temporal signal drift (due to diffusion-limited O_2 consumption at the sensor), probe fouling, electromagnetic interference, and lower sensitivity (i.e., low detection limit) in low-O_2 environments constitute the main disadvantages of polarographic electrodes (Table 1; refs. [28,56,59]). Probe miniaturization and the introduction, development and establishment of the self-referencing modality mitigated these problems[56,60–64] but did not discourage the research of concurrent and improved alternatives.

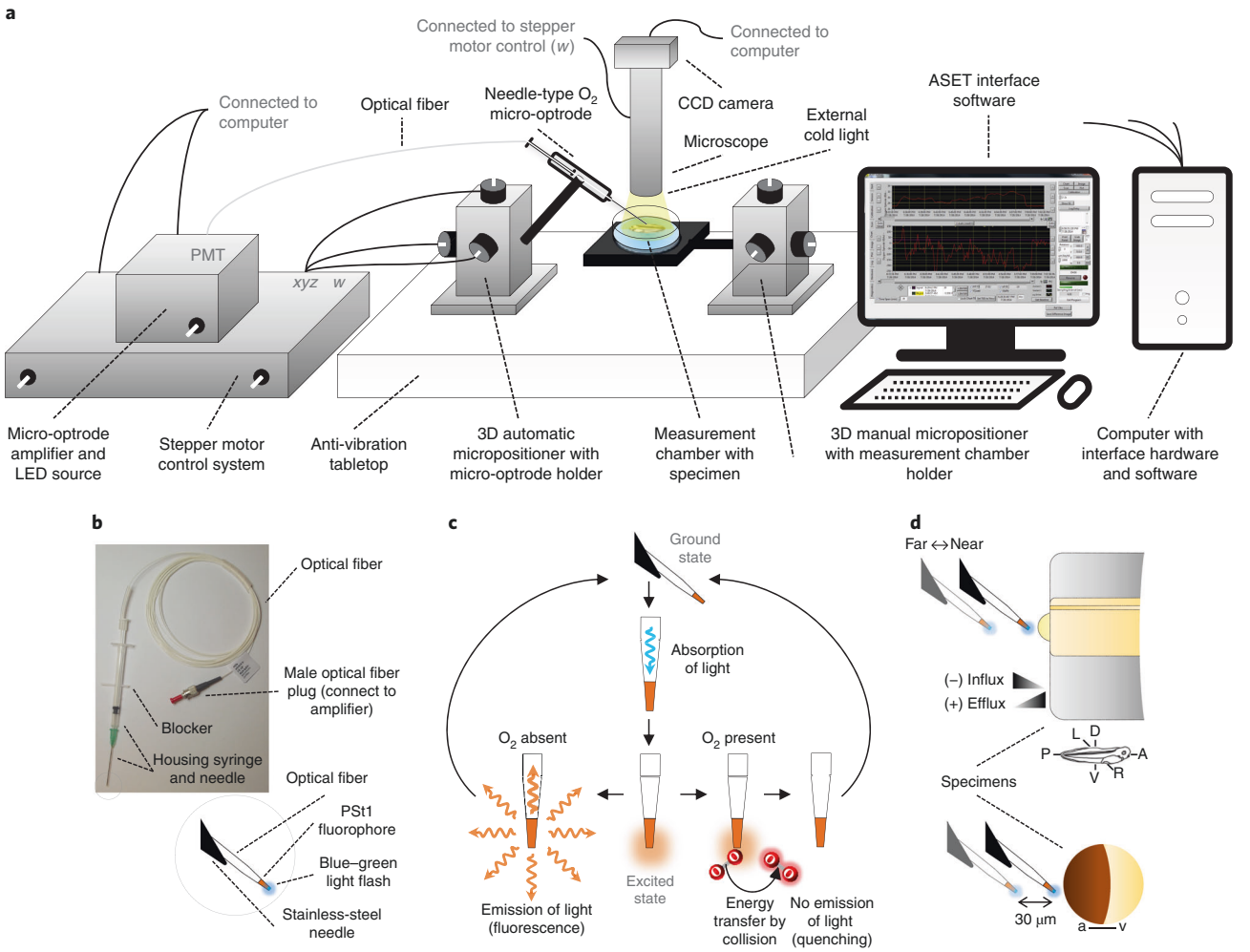

Fig. 1 | Scanning micro-optrode technique (SMOT). a, Schematic representation of the SMOT system and circuitry. A pulse of fluorescent light travels down the optical fiber and then travels back up the fiber, where its signal is converted to an electronic signal by the photomultiplier tube (PMT) housed in the micro-optrode amplifier. **b**, Needle-type oxygen-specific micro-optrode. A tapered glass optical fiber with a tip diameter of <50 µm is housed in a stainless-steel needle 40 mm long and with a 0.8-mm outer diameter. The blocker is an adaptation in the syringe to hold and protect the micro-optrode inside the needle after use. Inset: schematic depiction and detail of the oxygen-sensitive sensor tip with the coated PSt1 fluorophore (solid-state matrix). **c**, Schematic of the fundamentals of the fluorescence quenching-based oxygen measurement by SMOT (details in Box 1). **d**, Experimental design of representative specimens (two most used by us to test the system). Top, *X. laevis* tadpole tail; bottom, *X. laevis* oocyte. Details of near (full-color) and far (semi-transparent color) positions of micro-optrode during excursion. Negative values are net influx and positive values are net efflux. Tadpole tail scheme (lateral view) is displayed in the same orientation as the whole organism anteroposterior (A–P), dorsoventral (D–V) and left–right (L–R) axes (middle scheme). The oocyte scheme (lateral view) is displayed in the animal (a) to vegetal (v) pole orientation. Sizes in schemes are relative and proportional approximations, except for the computer, which is zoomed out, and the micro-optrode, which is zoomed in for clarity.

Limitations of the approach

Depending on the application, some advantages of the approach may inadvertently become a limitation. A clear example is the higher spatial resolution of micro-optrodes, which permits the pinpointing of O_2 fluxes in a fraction of a cell. However, if the goal is to map a large part of the cell or tissue simultaneously upon treatment, then imaging methods may be more suitable than the technique herein described.

Because the micro-optrode is housed in a needle, it allows the researcher to safely impale the micro-optrode into readily accessible or superficial tissues (e.g., solid tumors), organs (e.g., skin and eye) or body fluids (e.g., blood). However, deeper or fragile tissues or organs (e.g., bone tumor, heart and brain) may be out of the impalement range without further invasive surgery. Isolation of the tissue/organ of interest (ex vivo assays) from the organism may be required to overcome the accessibility limitation.

Table 1 | Advantages and disadvantages of oxygen flux measurement with micro-optrode vs. polarographic microelectrode

Property[a]	Micro-optrode	Polarographic microelectrode
Sensing mechanism	Collisional (or dynamic) fluorescence quenching by O_2	O_2 chemical reduction at 0.7 V
Temporal resolution	11 s for single micro-optrode[b]; 2 s for dual micro-optrode[b]	<1 s
Spatial resolution (ø)	<50 µm (probably will increase)[c,d]	~5 µm (typically lower, ~30 µm)
Sensitivity	Picomole	Picomole
Resolution	0.01%	0.01%
Reference electrode	No	Yes
Temperature-sensitive	Yes. Operates in the 0–50 °C range, requiring temperature compensation if varying temperature. According to manufacturer, a ±0.2 °C increase results in pO_2 ±0.15% shift	No. Operates at temperatures of up to ~200 °C
Electric and magnetic interference	No. Based on light, not electrical properties	Yes. Need of a Faraday cage and careful grounding
Chemical interference (cross-sensitivity)	None or limited. Interference by chlorine gas and organic solvents	Yes. Interference by chlorine, ozone (O_3), nitrogen oxide and hydrogen sulfide (H_2S) gases
Medium phase measurements	Liquid and gas phases	Liquid phase
Analyte (O_2) consumption	No	Yes
Reversibility	Yes. Fully	None or limited. Chemistry disturbance due to analyte consumption
Dual or multiple sensor	Yes. No distance requirements with a second micro-optrode or with a microelectrode	Yes. Requires ≥40-µm distance between microelectrodes[e]
Portability	Yes. At the expense of automation. Optical fiber allows remote reading	None or limited
Endurance	Long-lasting micro-optrode (if not mechanically damaged, no need for replacement for many years)	Long-lasting microelectrode
	Robust tip (break resistant)	Fragile tip (break sensitive)
	No fluorophore (solid state) leakage	Platinum tip ball does not leak
	Photobleaching (very slow and readily overcome by recalibration)	No photobleaching
User-friendliness	High	Medium
	Micro-optrode ready-to-use	Microelectrode manufacture required
	Quick training	Medium training

[a]Extracted from refs. [32,35,43,49,52]. [b]Highly dependent on sampling rules (Box 3); temporal resolutions annotated are for the used sampling rules. [c]Micro-optrodes acquired had slightly varying tip diameters of <50 µm. For higher spatial resolutions, smaller tip diameters can be requested from the micro-optrode manufacturer. [d]Spatial resolutions as high as 5 µm have been reported in micro-optrodes made by researchers[47]. [e]Polarized microelectrodes generate a local electric field; therefore, a safe distance is required to avoid sensor crosstalk. This requirement is discarded if a second sensor is light-based, i.e., a micro-optrode.

Furthermore, the technique assumes that the sample or animal is immobilized to mitigate noise and to prevent artifactual recordings. Therefore, physical or chemical immobilization procedures are required, which may confer a limitation in certain experimental designs. However, this limitation is also shared by other available techniques.

Applications of the approach

The turnkey SMOT system, using a ready-to-use micro-optrode (Fig. 1; Box 1), as well as alternative systems for the measurement and study of oxygen dynamics, is currently in a number of laboratories generating physiologically reliable data, especially in plant models[43,45–47,49]. Systems are also used in non-biological studies, such as in metal corrosion[65]. With proper mounting, tuning and calibration, SMOT is a very versatile technique and easy to adapt to disparate laboratory environments and research goals. Commercially available micro-optrodes can take different, and even customizable, configurations (e.g., for flow-through recordings or to be incorporated into catheters), further increasing the versatility and potential uses of the technique. Moreover, the SMOT system can be readily adapted to incorporate perfusion, incubation and/or advanced imaging systems, if desired, broadening its scope of applicability even more.

Box 2 | Liquid versus gas phase measurement

An advantage of the micro-optrode over the polarographic microelectrode (Table 1) is that the micro-optrode can acquire measurements in the gas phase. Owing to research purposes and specimen constraints, we measured all samples in the liquid phase; however, we successfully tested this possibility in a wounded diabetic mouse skin recording (figure). Note the similar plateaus after flux stabilization (liquid phase: −46.90 ± 0.71; gas phase: −50.45 ± 1.60; $P = 0.09$ (unpaired Student's t test, two-tailed P value)). For more robust and reproducible data collection, the airflow surrounding the measuring chamber must be markedly limited, and the humidity must also be controlled.

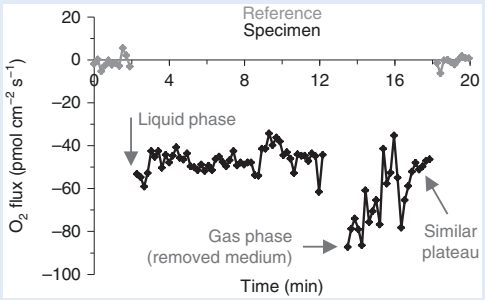

In our laboratory, we set up a 'Bioelectric and Redox Sensor Facility', with the micro-optrode sensor (together with microelectrode-based sensors) at its core, mainly to study animal wound healing and regeneration, but also other physiological phenomena. Recently, we carried out research, successfully applying this technique to study the O_2 dynamics during *X. laevis* tadpole tail regeneration[24]. Representative and comprehensive examples of this and other research are presented in the Anticipated results section.

In addition to its non-invasive capabilities, the micro-optrode has invasive potentialities in the static mode of measurement ('Experimental design' section). The metal needle can easily impale disparate tissues/organs, injecting the micro-optrode into previously inaccessible measurement regions. Examples that we are testing include reading intravenous pO_2 in rat tail and intraocular pO_2 in non-human primate (Supplementary Fig. 1a,b). Replacing the needle, a broken pulled capillary can provide a hole for the micro-optrode itself. We are testing this to measure intratissue pO_2 in the tadpole regeneration bud (Supplementary Fig. 1c). Furthermore, the micro-optrode itself can impale softer samples. Researchers can adapt these potentialities and apply them in their fields with relative ease. We also applied the micro-optrode successfully in a gas phase measurement (Box 2), an advantage over the polarographic microelectrode (Table 1) that demonstrates the micro-optrode's versatility and widens its usability.

Many other applications and potentialities for the micro-optrode exist, either in biological or non-biological contexts, for example, manure, sediment and biofilm profiling; package control; metal corrosion; and many others too numerous to test or list here (see the micro-optrode manufacturer's large database: www.presens.de/knowledge/publications).

Experimental design

Single micro-optrode mode

The standard mode of acquisition relies on the excursion (distance traveled by the sensor from near to far poles) of a single micro-optrode fully operated by the interface software (Automated Scanning Electrode Technique (ASET); Fig. 1d). At the first calibrations in the in-house system, the obtained values should be compared against and should fall within the manufacturer's calibration range, provided in the micro-optrode inspection sheet (Fig. 2a–c). After this verification, the system should be validated using artificial and natural sources and sinks (Fig. 2d–i). If the exponential/logarithmic relationship between flux and distance to sink is significant, then the system is efficient for experimental measurements.

Before data acquisition, preliminary preparation is typically required to make appropriate measuring chambers; to fine-tune chemical and/or physical immobilization, test chamber and sample placement to allow sufficient degrees of freedom to the moving micro-optrode; and to adjust zoom scope(s) to the desired visualization and imaging, After adjustments, some preliminary data should be collected to optimize and test the acquisition sampling rules. We advise taking some time in setting

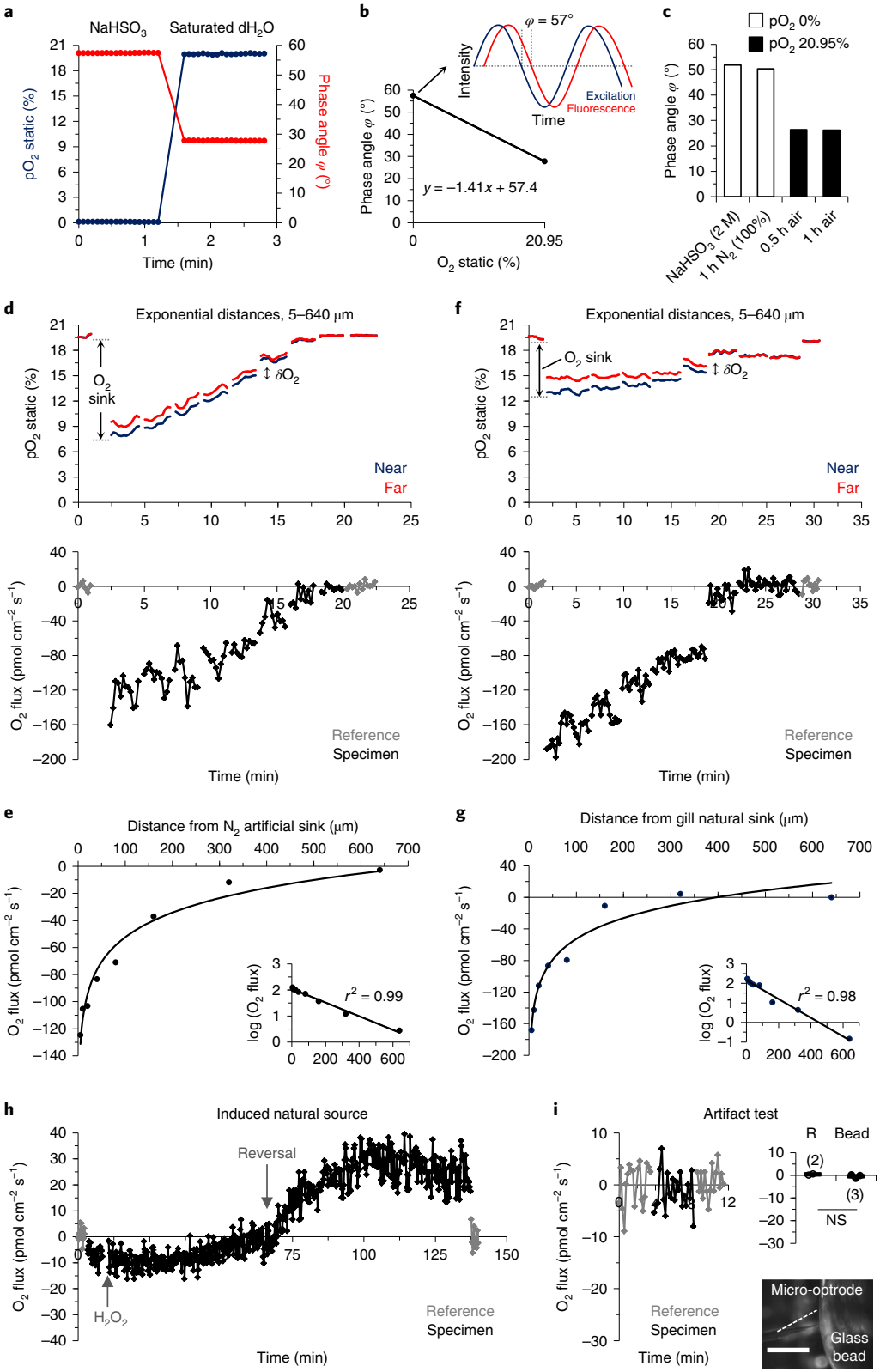

up the rules, because thereafter they should be kept unaltered for facilitated post-acquisition analysis. If the sampling rules are altered, some of the equations to derive O_2 flux must be updated (see details in Box 3 and the Supplementary Data).

The SMOT system is very versatile and contains module components (Fig. 1a,b); therefore, it is prone to modification for data collection in different animal models. In this protocol, we present data

◀ **Fig. 2 | Oxygen-specific micro-optrode calibration and validation. a–c**, Two-point calibration. Representative calibration readouts (**a**). Phase angle and pO_2 are inversely proportional (**b**). Inset, phase angle depiction. Different solutions and methods to achieve pO_2 0% and pO_2 20.95% yield similar calibrations (**c**). **d**,**e**, Artificial sink validation. Sink is a N_2 100% gas bubble at the tip of a broken pulled capillary. **f**,**g**, Natural sink validation. Sink is a gill of a stage 41 *X. laevis* tadpole. In **d**,**f**, top plots, pO_2 static measurements at near and far poles with annotated sink; bottom plots, O_2 flux calculated using the difference of near and far poles values (δO_2) from top plots (after conversion to O_2 concentration as detailed in Box 3). References and each distance (5, 10, 20, 40, 80, 160, 320 and 640 µm) from sink are delimited by a discontinuity in the solid lines; *x* axis labels in bottom plots also apply to top plots. **e**,**g**, O_2 flux as a function of the distance to the artificial (**e**) and natural (**g**) sinks fitted with an exponential curve. Insets, curves fitted to a linear regression after logarithmic (log) transformation, demonstrating exponential drop of flux with distance, as expected. **h**, H_2O_2-induced natural source validation. H_2O_2 at a final concentration of 1 mM was inoculated into the measuring chamber with an oocyte. Inoculation of H_2O_2 at 2 and 10 mM into inert glass beads did not induce a source of O_2 (not shown). **i**, Micro-optrode is artifact free. Inert glass beads do not have consistent fluxes. R, reference. Scale bar, ~0.5 mm. Data are presented using dot plots with mean lines. Statistical comparison was performed using the unpaired Student's *t* test (two-tailed *P* value). NS, non-significant. Number of biological replicates indicated in parentheses. All procedures involving animals were approved by the relevant institutional and national regulatory boards.

Box 3 | Sampling rule optimization for data acquisition in ASET

The interface software ASET (LV4) allows the user to optimize the sampling rules for data acquisition to obtain an improved signal-to-noise ratio. Important adjustable settings are the following:

(i) *Excursion*, distance traveled by the micro-optrode per iteration (near to far poles) (Fig. 1d). Typically, small-sized and/or low-gradient specimens might require smaller excursions, which can be increased in larger and/or high-gradient specimens. Usually, excursion is within 10–100 µm; 10 µm is a good starting distance for optimization of a new specimen type. Optimization in 5- or 10-µm steps is recommended. The excursion distance is entered into the flux calculation (Box 4); thus, if excursion is changed, the equation must be updated.

(ii) *Waiting time*, time that the program pauses after excursion to a new sampling locus, before acquiring an individual data point. This setting mitigates possible stirring artifacts due to micro-optrode movement. The automation (micropositioner and software) drives a smooth path with reduced velocity for the micro-optrode excursion, generating minimal, virtually negligible, liquid disturbance (frequencies slower than 0.5 Hz, as those in the micro-optrode, produce non-significant stirring artifacts[60]); therefore, this time can be very short. Optimization in 0.1-s steps is recommended.

(iii) *Sampling time*, time during which each data point is acquired, after the waiting time. The sensor is very sensitive; therefore, this time can also be short. Optimization in 0.1-s steps is recommended.

There is a tradeoff between the sampling rules and the sampling interval; larger excursion and times will increase the time to acquire a data point of flux. This tradeoff can also be taken into account during sampling rule optimization. In our recordings, we optimized the sampling rules to 1-s wait time, 0.5-s sample time and 30-µm excursion, which gave a sampling interval of 11 s (~0.1 Hz). Acquisition frequencies around this value are common[46,48,49] and yield a good signal. Once optimized, these rules can be kept unchanged in all measurements. The same or different rules can be applied for different types of specimens. Reference position was >>1 mm, generally ~5 mm, from the specimen surface; sample position was as close as possible, generally ~10 µm from the specimen surface. Fluxes were recorded for 2–5 min (~10–30 data points), usually enough for a consistent signal to be averaged (Box 5).

from lower and higher vertebrates. Moreover, the imaging capabilities can be updated according to the research needs. Some of the microscope (e.g., Dino-Lite digital microscope) function can be integrated into the ASET software interface, avoiding the simultaneous operation of multiple software programs.

Dual micro-optrode mode

To explore further the technique, we tested and validated an important experimental design using two ASET-controlled micro-optrodes simultaneously (dual micro-optrode mode; Fig. 3a). The new design markedly increases the temporal resolution of the system from 11 s (due to the microstepping plus the time required to acquire individual data points, both without generating stirring artifacts) to 2 s (for the used sampling rules; Table 1; Box 3), owing to the alternate flashing instead of excursion (Fig. 3b–d).

The dual micro-optrode mode has another substantial advantage over the single micro-optrode mode, which is its inherent potentiality to simultaneously acquire data of disparate species, such as O_2 and protons (H^+), using different species-specific micro-optrodes (Fig. 3e–g). Other micro-optrodes emergently available measure carbon dioxide (CO_2; PreSens prototype) and hydrogen peroxide (H_2O_2) (ref. [66]). Such experimental design expedites data acquisition and reduces animal numbers. A disadvantage of the dual micro-optrode mode is that the positioning of the two micro-optrodes exactly 30-µm apart (to mimic the excursion of the single micro-optrode mode and to use in the

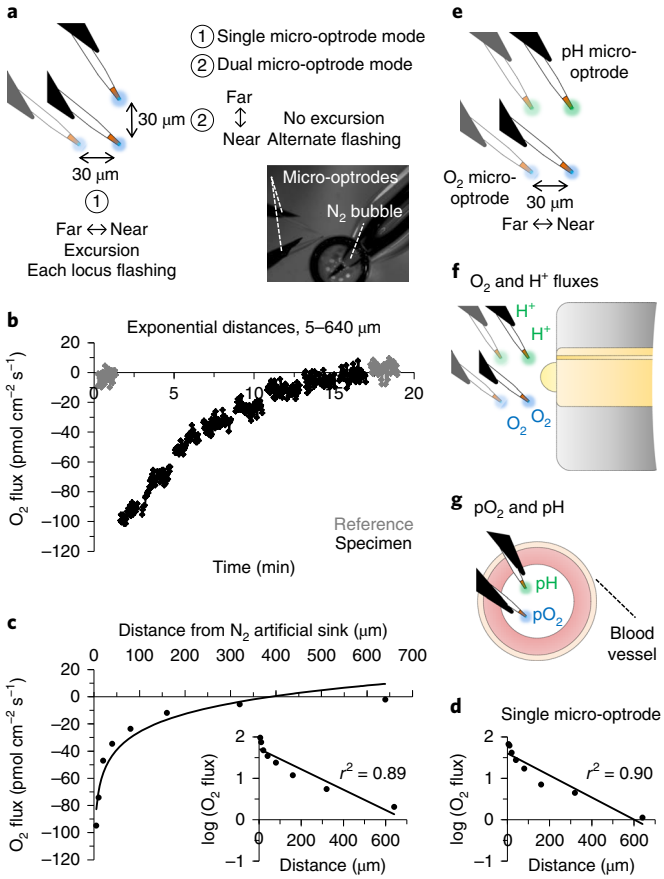

Fig. 3 | Dual micro-optrode mode. a, Schematic representation of the setup for dual micro-optrode measurement, as compared to that for single micro-optrode mode. **b**,**c**, Validation of the dual micro-optrode mode using an N_2 artificial sink. O_2 flux as a function of the distance to the sink. References and each distance (5, 10, 20, 40, 80, 160, 320 and 640 µm) from sink are delimited by a discontinuity in the solid lines (**b**). Fitting of an exponential curve (**c**). Inset, curve fitted to a linear regression after logarithmic (log) transformation, demonstrating exponential drop of flux with distance, as expected. **d**, Values were similar to single micro-optrode mode measuring the same N_2 bubble, further validating the dual mode. **e**–**g**, Potentialities of the dual micro-optrode. **e**, Dual micro-optrodes for pO_2 and pH operating in the near and far excursion mode. **f**, Non-invasive simultaneous measurement of endogenous fluxes of O_2 and protons (H^+). pH micro-optrode flashing color is pseudocolored green for distinction (actual light used is blue). **g**, Invasive simultaneous measurement of endogenous intratissue pO_2 and pH. Dual micro-optrodes operating in the static mode. Scheme is a transverse section of a blood vessel (e.g., from heated rat tail).

post-acquisition calculations) and in the same focal plane is relatively complicated to achieve. However, this is will probably be a one-time difficulty because the configuration can be kept and saved if several micropositioners and micro-optrodes are available. This disadvantage applies only when measuring flux of the same species (e.g., just O_2).

Static micro-optrode mode

The aforementioned single and dual modes are dynamic; i.e., they rely on excursion and alternate flashing of the micro-optrode, respectively. Alternatively, the single/dual micro-optrode can be used in the ASET-controlled static mode of acquisition, i.e., setting the excursion value to 0 µm in the interface software. Instead of generating a differential value from the O_2 gradient detected (converted into fluxes in downstream analysis), this mode reads the pO_2 at the local point. Depending on the research needs, the static mode can be selected over the dynamic mode, especially for invasive experimental designs. For instance, because the micro-optrode is housed in a stainless-steel needle with a 0.8-mm outer diameter, it can safely be used to impale a sample (the needle impales the sample first, then the micro-optrode is extended). We are currently exploring these applications by manually injecting the micro-optrode into the rat tail blood vessel (after heating the tail to ~40 °C to expand the vessel) or into non-human primate eye chambers (ex vivo) (Supplementary Fig. 1a,b). Furthermore, for smaller samples, a pulled glass capillary with the tip broken (similar to that used in oocyte

wounding) can be used to make a temporary hole through which the micro-optrode can impale a soft and fragile tissue, such as the tadpole tail bud tested during regeneration (Supplementary Fig. 1c). Because the micro-optrode (optical fiber) itself is sufficiently break resistant and sharp, we expect that it can also be used to directly impale samples.

Additional data acquisition modes

The single and dual micro-optrode modes are typically operated as manual linear scans. However, automatic 2D and 3D line and grid scanning can be pre-programed in the ASET software to automatically profile an immobile sample, depending on research needs and specimens used. We tested and used these modes successfully in enucleated rat eyes, because of their perfect immobilization. The automation can be extended to other animal models, provided sufficient chemical and/or physical immobilization is used, especially over longer periods of time. Interestingly, remote control of the software is also possible. Such modes are advised if productivity and efficiency are improved.

Moreover, photomicrographs and real-time or time-lapse videos are also potential modes of data acquisition that can be fully controlled by the ASET. These imaging data can be recorded simultaneously with numerical data, allowing important cross-comparisons.

Finally, the micro-optrode can be used in the gas phase. Experimental design and procedure are relative to liquid phase measurements, owing to research aims and to technical and specimen specifications. However, we tested the gas phase capability in a wounded diabetic mouse skin (Box 3). If this approach is followed, additional precautions to must be taken for confident data collection. The airflow and humidity surrounding the measuring chamber should be monitored and controlled to markedly mitigate the dissipation of O_2 gradients and ensure data reliability across different times/experiments (e.g., cover the rig or use an enclosing chamber, and use a humidity probe).

Materials

Biological materials

! CAUTION Any experiments involving live animals must conform to the relevant institutional and national regulations. The experiments shown in this protocol using tadpoles were approved by the Marine Biological Laboratory (MBL; protocol no. 14-59) and the University of California (UC), Davis Institutional Animal Care and Use Committee (IACUC; protocol no. 18601). The procedures using rodents were approved by the UC Davis IACUC (protocol nos. 16766 and 17876) **▲ CRITICAL** The examples shown in the Anticipated results section of this protocol are listed below. In addition, we have tested rat tail and enucleated non-human primate eye (gifted by the California National Primate Research Center), and we anticipate that our protocol will be compatible with in vivo and ex vivo tissues or organs readily accessible to the micro-optrode (ideally, in a minimally or non-invasive way). The protocol cannot be used in vivo on deeper or very sensitive tissues or organs, unless an invasive surgery is performed with utmost care.

- *Xenopus laevis* (Daudin, 1802) oocytes (Xenopus 1, cat. no. 12004) and tadpoles (National Xenopus Resource (NXR), cat. no. NXR_0031; or Xenopus Express, cat. no. TAD)
- *Mus musculus* (Linnaeus, 1758) skin from 8-week-old, male, BKS.Cg-*Dock7*^{m} +/+ *Lepr*^{db}/J heterozygous (non-diabetic) and homozygous (diabetic) mice (The Jackson Laboratory, cat. no. 000642)
- *Rattus norvegicus* (Berkenhout, 1769) eye from 7- to 8-week-old, male, Sprague–Dawley rats (Envigo, cat. no. 002; or Charles River, cat. no. 400)

Reagents

- Deionized water (dH_2O)
- Sodium bisulfite (mixture of $NaHSO_3$ and $Na_2S_2O_5$; Sigma-Aldrich, cat. no. 243973) **! CAUTION** Sodium bisulfite causes acute oral toxicity and serious eye damage; it also causes acute aquatic toxicity. Avoid contact with skin and eyes; do not store near acids. Use personal protective equipment while handling.
- Compressed N_2 (gas) cylinder (100%) **! CAUTION** Compressed N_2 is a pressurized gas cylinder; it should be handled properly.
- Sodium chloride (NaCl; Sigma-Aldrich, cat. no. S7653)
- Calcium chloride dihydrate ($CaCl_2{\cdot}2H_2O$; Sigma-Aldrich, cat. no. 223506)
- Potassium chloride (KCl; Sigma-Aldrich, cat. no. P9333)
- Magnesium chloride hexahydrate ($MgCl_2{\cdot}6H_2O$; Sigma-Aldrich, cat. no. MN-9272)
- HEPES (Sigma-Aldrich, cat. no. H3375)

- Sodium hydroxide (NaOH; Sigma-Aldrich, cat. no. 221465) **! CAUTION** NaOH causes severe skin burns and eye damage. Avoid inhalation of the vapor or mist; store in acids/bases cabinet. Use personal protective equipment while handling.
- Dimethyl sulfoxide (DMSO; Sigma-Aldrich, cat. no. D2650) **! CAUTION** DMSO may be harmful if inhaled, swallowed or absorbed through skin; may cause eye irritation. Keep away from sources of ignition; avoid contact with DMSO-containing toxic reagents, because DMSO readily transports through the skin. Use personal protective equipment while handling.
- *N*-benzyl-*p*-toluene sulfonamide (BTS; Tocris Bioscience, cat. no. 1870)
- Hydrogen peroxide solution (H_2O_2 solution; 30% (wt/wt) in H_2O; Sigma-Aldrich, cat. no. H1009) **! CAUTION** H_2O_2 solution causes acute oral toxicity, skin corrosion and serious eye damage. It also causes acute and chronic aquatic toxicities; keep away from sources of ignition. Use personal protective equipment while handling.
- Paraformaldehyde (PFA; Sigma-Aldrich, cat. no. P6148) **! CAUTION** PFA causes acute oral toxicity, skin corrosion and serious eye damage. It also causes acute and chronic aquatic toxicities; keep away from sources of ignition. Use personal protective equipment while handling.
- 2,4-Dinitrophenol (2,4-DNP; Sigma-Aldrich, cat. no. D198501) **! CAUTION** 2,4-DNP is toxic if swallowed, upon contact with skin or if inhaled; it may cause damage to organs through prolonged or repeated exposure. It is very toxic to aquatic life. Use personal protective equipment while handling.
- Potassium cyanide (KCN; Sigma-Aldrich, cat. no. 60178) **! CAUTION** KCN is fatal if swallowed, upon contact with skin or if inhaled; it is very toxic to aquatic life, with chronic effects. Use personal protective equipment while handling.
- Sodium azide (NaN_3; Sigma-Aldrich, cat. no. S2002) **! CAUTION** NaN_3 is fatal if swallowed or upon contact with skin; it is very toxic to aquatic life, with chronic effects. Use personal protective equipment while handling.
- Compressed CO_2(gas) cylinder (100%) **! CAUTION** Compressed CO_2 is a pressurized gas cylinder; it should be handled with care.
- Artificial tear solution (BSS+; Alcon Laboratories, cat. no. 0065080050)
- Hair removal cream (Nair; Church & Dwight)
- Phosphate-buffered saline (PBS; Amresco, cat. no. E404)
- Ethanol (95% (vol/vol); EMD Millipore, cat. no. AX0441-03) **! CAUTION** Ethanol causes severe eye and moderate skin irritation, as well as respiratory tract irritation. It is a highly flammable liquid and vapor; store in flammables cabinet. Use personal protective equipment while handling.

Equipment

▲ CRITICAL The SMOT turnkey system can be divided into three subsystems: hardware, software and microsensor. The core components of the hardware are obtained via Applicable Electronics (www.applicableelectronics.com); the acquisition software is provided by Science Wares (www.sciencewares.com); and the microsensor is acquired from PreSens (www.presens.de). All components for the technique and measurements are listed below.

SMOT system, hardware

- Single-channel micro-optrode amplifier and LED source (OA-1), with built-in photomultiplier (PMT), the light-to-electric signal transducer (Science Wares)
- Computerized motion control, four-axis micro-stepper system (CMC-4), with programmable step, direction and speed. Fourth axis (*w*) is for microscope focus function (Applicable Electronics)
- 3D motorized micropositioners (Science Wares, model no. 3DMM) with extra focus motor
- Upright zoom scope (1–14× magnification) with motorized focus (75-mm travel) and long working distance (typically >5 cm; increase or decrease depending on sample dimensions; Applicable Electronics) These built-in optics can be readily and easily disassembled and substituted with a compound, upright, inverted or any other type of microscope without compromising compatibility with the acquisition software (ASET). The ASET-controlled motorized focus capability might be lost depending on the microscope.
- A horizontal zoom or other scope can also substitute for or be added to the built-in vertical zoom scope for further or enhanced imaging. In another SMOT system, we added a Dino-Lite digital microscope (AnMo Electronics, cat. no. AM4013MTL) horizontally oriented in some experimental designs. Imaging monitoring can be performed with the ASET software following the installation of an update.

- Color USB digital camera (1.3 megapixel; IDS μEYE, model no. UI-1240LE; www.en.ids-imaging.com) for image capture and time-lapse and real-time video acquisition
- Desktop computer: for best performance, it should have Windows 10, 64 bits, a minimum error-correcting code (ECC) RAM with 8 Gb, and a hard disk dual 1 Tb, 7200 r.p.m. in RAID 1 configuration
- Analog-to-digital (A/D) board (National Instruments (NI), cat. no. PCI NI-6229) with breakout box/cables
- Motion-control board (NI, cat. no. PCI NI-7332)
- Digital video interface (NI, cat. no. NI-IMAQ): allows the control of the USB digital camera via ASET upon a driver installation (www.sciencewares.com/downloads/aset-lv4)
- Liquid crystal display (LCD) flat-screen video monitors: two linked as extended screen, with one for acquisition software panel and another for sample visualization software panel
- Micro-optrode holder: assembled with stainless-steel mounting posts and post clamps (Newport, cat. nos. M-MCA-2, M-MSP-1 and M-MSP-2), and a syringe holder (Science Wares, cat. no. MOH2) mounted onto the 3D motorized micropositioners
- Second micro-optrode micropositioner and holder: small 3D manual micropositioner (Narishige, cat. no. M-44) with a syringe holder (Science Wares, cat. no. MOH1) mounted onto the 3D motorized micropositioners (only for dual micro-optrode mode)
- 3D sample holder: flat, square sample holder (Applicable Electronics) mounted onto a 3D manual micropositioner (Line Tool, model A), permitting high degrees of freedom for sample positioning
- Vibration-isolation active-air tabletop with M6 tapped holes (Kinetic Systems, model no. 2212), where micropositioners, scope and sample holder are mounted. Place the vibration-isolation tabletop onto a working table or bench. In another SMOT system, we use a heavy marble table topped with a metal platform with M6 tapped holes (Edmund Optics, cat. no. 55-251). Alternatively, another suitable anti-vibration table/tabletop can be used.

SMOT system, software and microsensor

- Automated Scanning Electrode Technique (ASET) interface software, v.LV4, LabVIEW application (Science Wares: www.sciencewares.com/downloads/aset-lv4). ASET comes with a full installer that installs LabVIEW and the drivers required to recognize and control the NI hardware for signal processing, motion, photography and video. This software entirely automates the SMOT system for data, metadata and imaging acquisition.
- Needle-type oxygen-specific micro-optrode (NTH-PSt1-L2.5-TS-NS20/0.4-NOP or NTH-PSt1-L5-TS-NS40/0.8-NOP). For the latter, the most used, a stainless-steel needle of 40-mm length and 0.8-mm outer diameter houses the tapered glass optical fiber with a tip diameter of <50 μm (PreSens, cat. no. 200000062 or 200000069, respectively). Alternatively, micro-optrodes can be manufactured in-house from pulled glass optical fiber with a fluorophore embedded in the tip as detailed elsewhere[43,45].

Additional equipment

- LED cold light source (Genesee Scientific, cat. no. 59-500) Alternatively, an optical fiber ring illuminator or another light source, compatible with the research needs, can be used
- Tabletop thermometer (RadioShack, cat. no. 63-1035)
- Aquarium air pump and airstone, with silicon tubing connection
- AC power line conditioner (Tripp Lite, model no. LC1800), with voltage regulation and surge protection, connected to local outlet
- Power strip with switch, connected to the AC power line conditioner and to which all equipment is connected

Equipment for experimental measurements

- Personal protective equipment (lab coats, gloves, goggles and masks), for the handling of and experimentation with harmful reagents/solutions
- Plastic Pasteur pipettes (5 ml; Globe Scientific, cat. nos. 137030 and 137018), for the sorting of oocytes and tadpoles, and for sample and media transfer
- Petri dishes (60 and 100 mm; Genesee Scientific, cat. nos. 32-105 and 32-107, respectively), for the sorting and manipulation of oocytes and tadpoles, and for the making of calibration, dissecting and measuring chambers
- Non-treated plates (6 well; Genesee Scientific, cat. no. 25-100), for tadpoles incubation
- Nylon mesh (800-μm pore size; Dynamic Aqua-Supply, cat. no. NTX750)

- Nickel–chromium wire
- Epoxy resin (VWR, cat. no. 500043-451)
- Glass pipette puller (Narishige, model no. PC-10)
- Straight microelectrode holders (Warner Instruments, cat. no. QSW-A15P)
- Borosilicate glass capillaries without filament (World Precision Instruments (WPI), cat. no. TW150-4)
- Glass beads (Sigma-Aldrich, cat. no. 18406)
- Biopsy punch (2 mm; Miltex, cat. no. 33–31)
- Scalpels (no. 10 blade, Feather Safety Razor; no. 15 blade, Henry Schein)
- Premier edge microsurgical knife (Oasis, cat. no. PE 3015-3)
- Fine spring scissors (Fine Science Tools)
- Acrylic cube with opening lid
- Silicon tubing and tubing adaptors
- N_2 flow meter regulator
- CO_2 pressure compensation flow meter (Western Medica, cat. no. M1-940-12FM)
- Magnetic stand (WPI, model no. 10), to hold the 3D manual micropositioner
- 3D manual micropositioner (WPI, model no. KITE-R), for the manipulation of the pulled glass pipette used to wound oocytes
- Temperature-control equipment (optional, depending on the experimental design) For example, temperature probes, heating pads, heated stages, temperature controllers, or even an enclosed environmental chamber. Temperature monitoring can be performed with the ASET software following the installation of an update.
- Dissecting microscope for the sorting of oocytes and tadpoles; glass pipette preparation; wounding of oocytes, tadpole fins and rat eyes; and for the amputation of tadpole tails
- Centrifuge tubes or Erlenmeyer flasks
- Glass capillary

Data analysis software

- Excel (Microsoft Office 2016: http://www.microsoft.com) for data analysis and visualization
- Template Excel worksheet (Supplementary Data) for automated data analysis and visualization
- ImageJ (v.1.47u; National Institutes of Health: https://imagej.nih.gov/ij) for image visualization and treatment (setting scale bars and measurement sizes)
- GIMP (v.2.8.16; The GIMP Development Team: https://www.gimp.org) for image visualization and non-manipulative editing (recolor, resize and crop)
- Prism (v.5.02; GraphPad Software: www.graphpad.com/scientific-software/prism) for inferential statistics

Reagent setup

▲ **CRITICAL** We routinely use the calibration solutions described below. The measuring solutions can be used instead of the standard dH_2O, because O_2 solubility is affected by salinity[67]. However, the media salinity levels used (as well as others routinely used in biological research) are too low to have any measurable effect on flux calculations. If the measurement medium composition is unknown (e.g., proprietary media) or if some components are known/suspected to chelate or otherwise affect ambient pO_2, we advise comparing calibrations using such medium to those using standard dH_2O. In the case of a consistent significant difference, calibrate the micro-optrode using the measurement medium. Note that the calibration relies on anoxic and normoxic pO_2; therefore, solutions made either with dH_2O or medium must have those O_2 concentrations. To guarantee this, a pre-calibrated micro-optrode can be used to assess the pO_2 of the calibration solutions under test. Alternatively, the calibration solutions can be prepared as recommended in the instruction manual of the micro-optrode manufacturer.

Anoxic (pO_2 0%) calibration solution

Prepare the saturated reducing agent (0.2 or 2 M sodium bisulfite (mixture of $NaHSO_3$ and $Na_2S_2O_5$) in dH_2O). The 0.2 and 2 M sodium bisulfite solutions remain anoxic for at least 6 months and 2 years, respectively, if properly stocked ! **CAUTION** Use appropriate protective personal equipment for the making and handling of the sodium bisulfite solutions ▲ **CRITICAL** To avoid solution oxygenation over time, keep the stock container tightly closed and with little to no air inside; however, surplus sodium bisulfite is an efficient anoxic buffer.

Alternative anoxic calibration solution
Anoxic solution may also be prepared by aerating ~20 ml of dH_2O for 30 min using an airstone connected to a compressed nitrogen gas cylinder (100% N_2 gas). If measuring solutions instead of dH_2O, use this procedure for the anoxic calibration of the micro-optrode **! CAUTION** The pressurized gas cylinder should be handled properly **▲ CRITICAL** A shorter aeration time might not generate a completely anoxic solution. The container can be a centrifuge tube (50 ml) or another type of container with a narrow entry (e.g., Erlenmeyer flask) **▲ CRITICAL** Use the O_2-purged solution immediately after preparation. The solution cannot be stored because it oxygenates quickly; e.g., in an open Petri dish (60 mm), pO_2 reaches ~1–4% at 5 min after aeration, ~15% at 10 min and ~19–20%—almost complete reoxygenation—at 30 min.

Normoxic (pO_2 20.95%) calibration solution
Aerate ~20 ml of dH_2O for ~20 min using an airstone connected to an aquarium air pump. If measuring solutions instead of dH_2O, use this procedure for the normoxic calibration of the micro-optrode **▲ CRITICAL** A shorter aeration time might not generate a completely saturated solution. The container can be a centrifuge tube (50 ml) or another container with a narrow entry (e.g., Erlenmeyer flask). Agitate the container or stir the liquid for <30 s to preclude a supersaturated solution **▲ CRITICAL** Use the air-saturated solution immediately after preparation. The solution cannot be stored because it will quickly reach a non-saturated equilibrium with local (container or environmental) atmosphere.

MMR stock and working solutions
Prepare a stock solution of 10× MMR (oocyte and tadpole media) by mixing reagents in dH_2O in the following concentrations: 1 M NaCl, 20 mM $CaCl_2{\cdot}2H_2O$, 20 mM KCl, 10 mM $MgCl_2{\cdot}6H_2O$ and 50 mM HEPES. Adjust the pH to 7.1–7.2 with 1 M NaOH (pellets dissolved in dH_2O). Sterilize by autoclaving and store at room temperature (21–23 °C) indefinitely. Prepare the working medium of 1× (oocytes) or 0.1× (tadpoles) MMR by 1:10 and 1:100 dilutions in dH_2O, respectively.

BTS stock and working solutions
Prepare a stock solution of 50 mM BTS (tadpole immobilizing solution) in DMSO and store aliquots at −20 °C for at least 1 year. Prepare the working concentration of 50 μM BTS by 1:1,000 dilution in 0.1× MMR.

H_2O_2 stock and working solutions
Prepare a stock solution of 1 M H_2O_2 in dH_2O and store at 4 °C. Prepare the working concentration of 1, 2 and 10 mM H_2O_2 (O_2 efflux inducer) by dilution in 1× MMR .

PFA solution
Prepare 4% (wt/vol) PFA by mixing weighted powder in pre-heated (60 °C) 1× PBS and store aliquots at −20 °C for up to 1 year.

Stock and working solutions for drugs
Prepare stocks for drugs 2,4-DNP (in DMSO), KCN and NaN_3 (in dH_2O) and store aliquots at −20 °C. Prepare working concentrations of 50 and 100 μM 2,4-DNP, 1 mM KCN, and 2 mM NaN_3 by dilution in 0.1× MMR.

BBS+ stock solution
Prepare BSS+ (rat eye medium) by injecting the 20 ml from the Part II vial into the 480 ml of the Part I bottle, using the provided vacuum transfer device. Use within 6 h after preparation or store at 4 °C.

1× PBS
Prepare 1× PBS (mouse skin medium) by dissolving the tablets in dH_2O; store at room temperature indefinitely.

(Optional) micro-optrode cleaning and sterilization solutions
Prepare 3% (vol/vol) H_2O_2 by a 1:10 dilution in dH_2O of the bulk reagent or prepare 75% (vol/vol) ethanol by dilution of bulk ethanol in dH_2O. These solutions are optional, prepared depending on the experimental design.

Equipment setup

SMOT system setup

Our SMOT system is schematized in Fig. 1. SMOT is a turnkey system available from Applicable Electronics (www.applicableelectronics.com), which also provides loose parts and technical (pre-sential or remote) assistance. SMOT is entirely controlled and automated by the ASET software for sensor operation and for data, metadata and imaging acquisition. ASET fully operates the movement and activity of the micro-optrode acquired from PreSens. Of the two available sensor tip configurations, we acquired the tapered sensor tip, which best fulfils our research requirements and probably those of most physiological studies. Compared with the flat-broken sensor tip (diameter of 140 µm), the tapered sensor has higher spatial and temporal resolutions but lower robustness and light stability (higher photobleaching) and higher signal drift. The spatial resolution of the SMOT system is dependent on the micro-optrode tip diameter (<50 µm). If required, the micro-optrode manufacturer (PreSens) might select probes with elevated spatial resolution. The temporal resolution of SMOT is dependent on the sampling rules (Box 3) but can be up to 2 s. Importantly, SMOT can be integrated with other systems to allow simultaneous measurements (using multiple sensors) of disparate phenomena, including (but not limited to) electric currents, potentials (both membrane and transepithelial), ion fluxes, pH and H_2O_2 concentration. Some of these potentialities are expanded below. Indeed, Applicable Electronics offers a service to integrate most of these techniques within the same physical and digital environment. Moreover, the ASET interface software can be readily programmed and customized (on demand) to integrate such disparate data recordings.

Other companies that provide complete sensor systems, parts and accessories include (but are not limited to) PreSens (www.presens.de/products/o2) and WPI (www.wpiinc.com/product-listers/oxygen-sensors). In addition to the mentioned micro-optrode, PreSens commercializes the amplifier/meter (e.g., Microx 4) and the interface software (e.g., Datamanager). WPI commercializes the amplifier (e.g., OxyMicro), the micro-optrode (e.g., MicroTip) and the interface software (e.g., OxyMicro Software). Younger USA (www.youngerusa.com) commercializes a turnkey microelectrode-based system (Non-invasive Micro-test Technology; e.g., NMT100) with interface software (e.g., Non-invasive Ion & Molecule Flux Measurement Software), into which a third-party micro-optrode can probably be integrated.

Calibration chambers

Calibration chambers are unaltered 60-mm Petri dishes half-filled with the anoxic and normoxic solutions.

Dissecting/measuring chamber (oocytes)

The dissecting/measuring chamber for oocytes is an in-house-made chamber consisting of a 60-mm Petri dish with an ~1 cm^2 nylon mesh glued with epoxy resin to the center of the dish bottom. The mesh holds the oocytes immobile during measurements and during wounding with a pulled and broken-tip glass pipette[24,68]. Half-fill the dish with 1× MMR supplemented with different reagents (fixative or drugs) according to the experimental conditions.

Dissecting chambers (tadpoles)

The dissecting chambers for tadpoles are unaltered 60-mm Petri dishes. For tadpole fin wounding and half tail amputation, use a 2-mm biopsy punch and a no. 10 scalpel blade, respectively. Half-fill the dishes with 0.1× MMR supplemented with 50 µM BTS for chemical immobilization[21,24].

Rodent euthanasia chamber

The rodent euthanasia chamber is an acrylic cube with an opening lid, connected with silicon tubing to a fixated CO_2 (gas) cylinder attached to a flow meter regulator. For rats and mice euthanasia takes ~5–10 min; death should be confirmed with cervical dislocation, according to local IACUC guidelines[69].

Dissecting bench (rodents)

Tape an ~50 cm × 50 cm piece of coated paper to a laboratory bench for enucleation of rat eyes with fine spring scissors or for mouse skin wounding with a no. 15 scalpel blade. The square surface should be cleaned and sterilized with 75% (vol/vol) ethanol before and after procedures[69].

Measuring chamber (tadpoles)
The in-house-made measuring chamber consists of a 60-mm Petri dish with an ~10 × 2-mm plastic strip placed on a small plastic square (provides height to facilitate probe access), which is welded (with melting plastic) to the center of the dish bottom. The strip holds the tadpole immobile (chemically immobilized with BTS) during measurements. The chamber is half-filled with 0.1× MMR supplemented with 50 µM BTS for chemical immobilization and additional reagents (drugs) according to the experimental conditions[21,24].

Measuring chamber (rat eyes)
This in-house-made chamber consists of a 60-mm Petri dish with two wire loops glued with epoxy to the dish bottom. The wire loops end in small-diameter circles (at the center of the dish) that immobilize the eyeball during measurements and corneal wounding by scraping ~2 mm^2 of the epithelium with a microsurgical knife. Half-fill the chamber with BSS+[69,70].

Measuring chamber (mouse skin)
This measuring chamber is an unaltered 100-mm Petri dish half-filled with 1× PBS.

Measuring chambers (all)
We usually cut a piece of the 60-mm Petri dish edge to increase the degrees of freedom of the moving micro-optrode. If required, the chamber can be sterilized, adapted and/or treated for microscopic or other experimental design specifications. Common examples include the replacement of the plastic bottom with a light-friendly glass patch, coating with fibronectin and sterilization by ultraviolet light.

Procedure

Micro-optrode calibration ● Timing 30 min plus (one-time) 15 min to make the pO_2 0% solution

▲ **CRITICAL** Calibration of the micro-optrode is done with a conventional two-point calibration of dissolved pO_2 values of 0 and 20.95% (Fig. 2a–c). Calibrations should be bracketed by the calibration value range provided in the manufacturer's inspection sheet for the acquired micro-optrode. After extensive use, values may normally differ (see also Step 27). Alternatively, the calibration can be performed as recommended by the instruction manual or video tutorial of the micro-optrode manufacturer (www.presens.de/support-services/videos).

1 Set the experimental temperature in the ASET software.
▲ **CRITICAL STEP** Temperature affects O_2 diffusion[71] and is a parameter inserted into the equations to derive the O_2 flux value (Box 4). Moreover, the micro-optrode is temperature sensitive; therefore, temperature during calibration should be the same as during measurements for data accuracy.
▲ **CRITICAL STEP** We typically verify and set the temperature each time at the beginning of calibration because laboratory rooms commonly have a negligible temperature variation. For alternative amplifiers with built-in temperature compensation (temperature sensor to offset variation), this step is not needed.
? TROUBLESHOOTING

2 Extend the micro-optrode from the housing needle by removing the protectives cap and blocker from the syringe and pushing the plunger.
▲ **CRITICAL STEP** To prevent breaking of the sensing tip, first immerse the needle in dH_2O for 5–10 min before extending the micro-optrode. This is to dilute and wash away any possible salt crystals or other debris remaining inside the needle from previous use.
? TROUBLESHOOTING

3 Half-fill a Petri dish with the pO_2 0% (anoxic) calibration solution, immerse the micro-optrode (avoid immersing the needle) and wait 1 min for stabilization. Acquire the phase angle of the fluorescence signal using the 'Calibration' tab in ASET.
▲ **CRITICAL STEP** The micro-optrode is temperature sensitive; ensure that the setup is calibrated with calibration solutions that are at the same temperature as the desired experimental temperature.
▲ **CRITICAL STEP** If the intended measurements will be gaseous (in air) instead of dissolved pO_2 (in liquid), then calibrate in the gaseous state (100% N_2 (gas) and atmospheric pO_2 20.95%; also see Box 2).
? TROUBLESHOOTING

Box 4 | Stepwise flux calculations

For each new experiment, the ASET program creates, by default, two comma-separated value (.csv) files compatible with Excel: one stores exclusively raw data, and the other stores metadata (such as calibration details and imaging times) and annotations (log entries). Both files are saved automatically and continuously until the end of the experiment. Using the calibration and phase angle shift of acquired data, the ASET software automatically calculates and saves raw data as percentage pO_2 (Box 1). The data and information from the program files are then extracted to an in-house-developed worksheet template (Excel file), pre-loaded with automatic formulas and plots in series, to calculate and visualize O_2 percentages, concentrations and fluxes in ~1 min in few steps (Supplementary Data). For our research purposes, the worksheet is optimized to calculate O_2 fluxes; however, with some modifications and the use of conversion equations, it can be adapted to calculate, for example, air saturation. A useful 'Oxygen Unit Calculation' (conversion) sheet is available from the micro-optrode manufacturer (www.presens.de/support-services/download-center/tools-utilities).

The O_2 flux—net O_2 molecules moving through a determined area over a time period—with or without a biological barrier (i.e., cell membranes, tissue/organ epithelia or organism integuments) follows passive diffusion in a supply–demand way, being physically described by Fick's first law of diffusion. The flux magnitude and flux direction are driven by local gradients, which in turn are generated by cell function and behavior, such as cellular respiration, signaling, proliferation, migration and apoptosis, as well as cellular response to bacterial infection (oxidative burst) and exogenous bio-physical/chemical stimuli. The micro-optrode reads out the sum of this underlying O_2 physiology; however, until the final flux is derived, serial steps are taken as follows, starting with the computation of O_2 concentration.

The O_2 concentration, at near and far poles relative to sample, is calculated from percentage pO_2 (ASET raw data), using the following adapted[45] equation:

$$[O_2](\mu M) = \frac{p_{atm-pw(T)}}{p_N} \times \frac{\frac{pO_2}{0.2095}}{100} \times 0.2095 \times \alpha(T) \times 1,000 \times \frac{1}{V_M}, \quad (4)$$

where $[O_2]$ is the oxygen concentration (μM); p_{atm} is the atmospheric pressure (1,013.25 mbar at sea level); $p_W(T)$ is the vapor pressure of water (26.507 mbar at 22 °C (mean room temperature)); p_N is the standard atmospheric pressure (1,013.25 mbar); $\frac{\frac{pO_2}{0.2095}}{100}$ is the ratio of O_2 in the gas mixture (referred to elsewhere[45] as Q); 0.2095 is the volume content of oxygen in air; $\alpha(T)$ is the Bunsen absorption coefficient (29.908 $cm^3(O_2)$ cm^{-3} at 22 °C) and V_M is the molar volume (22.414 liters mol^{-1}). The temperature-dependent parameters $p_W(T)$ and $\alpha(T)$ are calculated/obtained using standard curves/tables consulted in the micro-optrode manufacturer's instruction manual. If the temperature changes, these parameters must be updated.
The $[O_2]$ value is then converted to picomoles per cubic centimeter by a net 1,000 factor multiplication and included in Fick's first law to calculate the fluxes:

$$J_{O_2}\,(\text{pmol cm}^{-2}\,\text{s}^{-1}) = -D \times \frac{\delta O_2}{\delta x}, \quad (5)$$

where J_{O_2} is the oxygen flux (picomoles per square centimeter per second), D is the diffusion coefficient of dissolved O_2 (2.42×10^{-5} cm^2 s^{-1} at 25 °C[78]), δO_2 is the concentration difference (picomoles per cubic centimeter) and δx is the excursion (0.003 cm).
The analyzed data are now in flux units. The reference is averaged and subtracted from each specimen flux data point. Finally, specimen flux is averaged to provide a single flux value per sampling locus (ROI). Negative values mean net influx (O_2 entering the animal tissue) and positive values mean net efflux (O_2 exiting the animal tissue).

4 Discard the solution and rinse the micro-optrode with dH_2O. When using 2 M sodium bisulfite, the solution can be saved into a new container for reuse. Do not reuse often (not more than 5–10 times), because the O_2 buffering capacity of the solution decreases with each new contact with atmospheric air (either by opening of the container or during the new calibration).

5 Repeat Steps 3 and 4 for the pO_2 20.95% (normoxic) calibration solution.
? TROUBLESHOOTING

6 Save the calibration measurements. The two-point calibration curve and linear slope are automatically calculated and incorporated by the ASET software to instantaneously derive pO_2 values and gradients during measurements (Box 4).
▲CRITICAL STEP One-time calibration is enough for at least a day of measurements. We made a performance proof; i.e., we tested the calibration shift after a full day of measurements (for the case, 12 recordings of ~30 min each; discontinuous sensor illumination or flashing). Phase angle shifts before and after measurements were −0.02° for pO_2 0% and −0.3° for pO_2 20.95%. These differences are negligible; therefore, we usually calibrate each new day of measurements to promote repeatability and reproducibility. The manufacturer recommends recalibration after 8 h of continuous sensor illumination or >18,000 data points. If the micro-optrode is replaced, a new calibration is required.

Micro-optrode validation ● Timing 1.5 h

▲CRITICAL We recommend validating the micro-optrode with a conventional artificial sink, 100% N_2 (gas) (Fig. 2d,e). We further validate using a natural sink (tadpole gills; Fig. 2f,g) and an induced natural source (H_2O_2; induced in oocytes; Fig. 2h). Note that purchased micro-optrodes are validated by default

by the manufacturing companies; these steps are just a supplementary verification of the micro-optrode efficiency in the in-house system to promote repeatability and reproducibility.

7 The large O_2 gradient generated by the artificial sink permits the protocol user to test for a large signal-to-noise ratio, to determine the extracellular diffusion limit of O_2 and therefore to define the microenvironment in which physiological activities might happen (typically <1 mm; Fig. 2d–g).

8 Heat-pull a glass capillary using the puller and gently break the tip to increase its diameter (>50 µm).

9 Connect the 100% N_2 (gas) cylinder to the capillary using silicone tubing and tubing adaptors.

10 Mount the artificial sink capillary in a microelectrode holder attached to a micropositioner.

11 Immerse the micro-optrode and artificial sink capillary in a Petri dish filled with dH_2O.

12 Open the gas cylinder to pressurize the capillary until a N_2 bubble is formed in its tip. Let the sink gradient from the bubble stabilize for at least 5 min.

? TROUBLESHOOTING

13 Record (details below) and plot fluxes as a function of the distance (Fig. 2e). Theoretically, the anoxic sink generates a local chemical gradient driving O_2 influx. Empirically, if the sensor measures, in its excursion, a lower O_2 concentration near the bubble than far from the bubble, and if the difference is a net influx, then the micro-optrode is validated for its ability and efficiency to correctly detect the magnitude and direction of O_2 fluxes.

PAUSE POINT One-time validation is enough for each micro-optrode.

Data acquisition setup ● Timing 1–3 h

14 Define the sampling rules for data acquisition in ASET according to the target specimen (see Box 3 for a detailed description of the different sampling rules).

Experimental measurements ● Timing 30 min (one time) plus 5–45 min of preparation and 7–30 min of measurement per sample

15 Prepare the biological specimen according to the experimental condition (fixate and wound oocytes and tadpoles, amputate tadpole tails, enucleate rat eyes or wound mouse skin) and immobilize the sample in the specimen-specific, in-house-made measuring chamber[21,24,68,69]. Immobilization (physical and/or chemical) should not compromise normal physiological activity and should grant free access and sufficient degrees of freedom to the moving micro-optrode.

▲CRITICAL STEP Before or simultaneously with the acquisition of definitive experimental measurements, it is important to perform negative and positive experimental controls (with drugs known to abrogate (e.g., fixation) or modulate O2 dynamics (e.g., mitocondrial targets)) that will guarantee robustness of the acquired data (Figs. 4 and 5).

16 Let the specimen equilibrate to the desired temperature, in the case that temperature control is used. In our studies, the measurements are performed at room temperature; however, temperature can be set and monitored using widespread equipment (e.g., heating pads, heated stages, temperature controllers or an enclosed environmental chamber), according to sample, model and/or research needs. Such equipment can be integrated into the SMOT rig system, which also allows the connection of a temperature probe. The ASET software can be updated to monitor temperature during the experiment.

▲CRITICAL STEP The temperature used for the experimental conditions should be the same as during calibration (Steps 1–3).

17 Place the sample under the zoom scope, focus the camera on the region of interest (ROI) of the specimen and carefully immerse the micro-optrode in the chamber away from the specimen (>>1 mm) for reference (also known as 'blank', 'buffer' or 'background') measurements.

▲CRITICAL STEP The results of many artificial and natural sources and sinks demonstrate that 1 mm perpendicular to the sample is usually a safe distance at which gradients are resolved (Fig. 2e,g). Sometimes, owing to the geometry of the specimen, a longer perpendicular distance might be required. For that reason, we set our reference position to >>1 mm (typically ~5 mm).

? TROUBLESHOOTING

18 Let the medium stabilize for ~1 min. Optionally, press the 'Baseline' button in the 'Chart' tab of ASET to offset ('zerify') any residual gradient.

▲CRITICAL STEP The medium in the chamber must be still (without ripples) to prevent noise and the dissipation of extracellular gradients. An anti-vibration table mitigates mechanical vibrations. To guarantee mechanical isolation, ensure that the rig is not touching the walls of the room and

avoid proximity to freezers or other vibration-producing equipment. To guarantee airflow isolation, avoid proximity to an air conditioner exit or hoods. If avoidance of airflows is not possible, isolate (cover) the measuring rig. Even the slightest vibration might move light samples in the microscale, increasing noise and therefore the time to reach a stable reference signal.

19 Start recording (the probe starts vibrating) at the reference position using the 'Chart' tab of ASET. Record at the reference position until a stable plateau is reached. Usually, 10 data points or up to 2 min of recording are enough. Alternatively, press the 'Reference' button in ASET to save a one-time reference value that will be automatically subtracted from each specimen gradient value; this will save time in post-acquisition analysis but provides a less accurate baseline value (Box 4).
? TROUBLESHOOTING

20 Stop recording (the probe stops vibrating), move the micro-optrode near to the specimen and focus it in the *z* plane with the target ROI. With default settings, the velocity of the ASET-controlled microstepping does not cause meaningful medium disturbance. If settings are changed and/or disturbance occurs, let the medium re-stabilize.
? TROUBLESHOOTING

21 Position the micro-optrode ~10 µm away from and perpendicularly to the ROI surface, using the ASET-controlled microstepping.
! CAUTION The micro-optrode tip is fragile; thus, when near the specimens, move the sensor with caution and in small steps to avoid damaging or breaking the tip. Although fragile, for soft specimens (e.g., soft tissues), the micro-optrode tip is robust enough to withstand touching them and can even penetrate the samples without breaking.
▲ CRITICAL STEP To obtain the most accurate data and to maximize the signal recorded, especially in weak gradients, the micro-optrode should be positioned as close as possible and excurse perpendicularly to the ROI. If geometry or other constraints of the specimen or the experimental design do not allow this, note that the measured signal is reduced because of both the distance from and the angle to the ROI. If required, empirically derived correction factors for the distance- and angle-dependent loss of signal can be applied in post-acquisition data analysis to obtain closer to absolute values.

22 Start recording (the probe starts vibrating) at the ROI as in Step 19. Fine-tune the positioning in *x*, *y* and *z* and even in angle (micro-optrode rotation in relation to the ROI) to find the peak signal near the ROI. Usually, for a stable plateau, 10–30 difference data (flux) points over 2–5 min are enough. Note that a stable plateau might take longer to acquire when fine-tuning. Excursion is not expected to cause meaningful disturbance in local gradients, and therefore the so-called stirring artifacts are virtually absent (Box 3).
? TROUBLESHOOTING

23 Repeat Steps 20–22 for measurements at additional ROIs.
▲ CRITICAL STEP Occasionally, when moving to a new ROI or reference position, the first few points might not represent the maximum or correct signal because of disturbances in the medium generated by chamber/specimen/micro-optrode movement and new local gradients. We usually start recording once a new position is reached and then, if necessary, delete those initial data points in post-acquisition analysis. Alternatively, let the medium stabilize for up to 1 min and then start recording. This might increase the time for data acquisition, but it will decrease the noise in trace, saving time in data analysis.
▲ CRITICAL STEP We recommend refreshing the measuring medium (e.g., 25% refreshment) occasionally, especially if many (>5) consecutive recordings are made and/or large specimens are used, to account for (offset) medium evaporation and animal respiration. Typically, we refresh the medium before using a new specimen. However, if refreshment is performed during recordings, a new reference measurement must be acquired.

24 After measuring at all desired ROIs, move the micro-optrode back to a reference position (>>1 mm from the sample) and start recording the reference value. The plateau should return to the baseline of the initial reference in Step 19.
▲ CRITICAL STEP A reference reading can also be taken after each ROI is measured, especially if some treatment (e.g., wounding or inoculation of drugs) is performed during the experiment. However, the system is highly sensitive and does not require many reference traces to ensure sufficient data quality.
? TROUBLESHOOTING

25 (Optional) Additional data acquisition modes, different from the described manual linear scan (Steps 19–24), can be pre-programed in the ASET software, depending on research needs. For example, one can set 2D/3D line/grid scanning to automatically, and even remotely, profile an

immobile sample. In addition, one can take screenshots of plots and sample photomicrographs (simply select the 'Print Panel' and 'Grab Image' tabs of ASET, respectively). More complex real-time or time-lapse videos are also potential modes of data acquisition. All imaging can be recorded simultaneously with numerical data, allowing linking of specified fluxes to images/videos.

26 Repeat Steps 15–25 for additional technical and biological replicates or different biological species.

27 Rinse the micro-optrode with dH_2O and retract it into the housing needle by pulling the plunger. Place the protective cap and blocker on the syringe. Alternatively, the micro-optrode can be immersed in dH_2O overnight if it will be used, after recalibration, in the next day(s).

▲ **CRITICAL STEP** Each time a salty, sugary, dirty, viscous or semisolid solution or medium is used, the micro-optrode must be rinsed or even cleaned carefully to prevent salt crystallization and contamination in the housing needle. This is a hazard that can potentially break the micro-optrode sensing tip and jeopardize contamination-sensitive experiments. Our research did not require stringent cleaning or sterilization, but, if necessary, the needle-type housing micro-optrode can be cleaned with regular liquid soap and sterilized with 3% (vol/vol) H_2O_2 or 75% (vol/vol) ethanol. The micro-optrode should not be autoclaved because of the polypropylene syringe (the manufacturer can provide syringes with autoclavable housing if requested).

? TROUBLESHOOTING

■ **PAUSE POINT** Store the micro-optrode at room temperature and protected from light (housing needle shelters micro-optrode from light). According to the manufacturer's accelerated aging tests, the oxygen sensor chemistry of the micro-optrodes has proven to be very stable, working properly for >10 years of average use. Unintentional and repeated touching of tissues/materials may impact micro-optrode longevity. An indicator of micro-optrode malfunction, for example, owing to photobleaching or unnoticed breakage, is the calibration value drift. When they drift continuously without stabilizing, or when the obtained values are very different in relation to the original calibration (performed in-house, not by the manufacturer), then micro-optrode replacement is advised.

Data analysis ● Timing 1–2 h (one time) for Excel template setup; ~7–16 min for extraction of data and analysis

28 Extract the raw data from the ASET program and analyze them using Excel. We use an in-house-developed worksheet template (Excel file) pre-loaded with automatic formulas and plots in series to calculate and visualize O_2 percentages, concentrations and fluxes in ~1 min in a few steps (available as the Supplementary Data). See Box 4 for a detailed description of the data analysis procedure.

29 Perform statistical analysis as appropriate, for example, paired Student's *t* test to quantitatively compare different experimental conditions. The statistical analysis used in this protocol is detailed in the figure captions.

Troubleshooting

Troubleshooting advice can be found in Table 2.

Table 2 | Troubleshooting table

Step	Problem	Possible reason	Solution
1	Signals in same-day/same-sample conditions are too disparate	Temperature change or fluctuation	Recalibrate the micro-optrode at the different temperature; set a new temperature in the ASET software at calibration
2	No signal	The sensor tip is broken	Acquire a new sensor or pull and re-coat the used sensor with a fluorophore[43,45]. Avoid salt crystallization or trapped debris inside the needle by careful rinsing with dH_2O after use
3	Low calibration phase angle for pO_2 0%	The calibration solution has been exposed to air	Make new pO_2 0% solution, minimize air exposure time and keep the stock container tightly closed
5	High calibration phase angle for pO_2 20.95%	Unsaturated calibration solution	Aerate for no less than 20 min
12	Continuous bubbling of N_2	Opening of the capillary is too large or flow meter allows too much pressure to reach the capillary	Make a new capillary with a smaller tip diameter or reduce the pressure in the flow meter

Table continued

Table 2 (continued)

Step	Problem	Possible reason	Solution
17	Ripples in the medium	Manual zooming, generating mechanical vibrations in the system	Use automatic ASET-controlled zooming (*w* motor microstepping), which prevents mechanical vibrations. If using alternative scopes, also try to use automatic zooming (e.g., via joystick)
19	Unstable reference	The optrode was too close to the sample	Increase the distance to at least ≥0.5 mm
20	Unstable signal and/or high noise	The medium and/or sample was disturbed	Allow stabilization (~1 min) of the medium. Move or isolate the SMOT system rig from mechanical vibrations and airflow
22	Compromised sample/ experiment	Soft tissue disruption by micro-optrode touching or micro-optrode is broken	Prepare a new sample or acquire a new micro-optrode. When close to the sample, reduce motor microstepping to 5–20 µm/ step to prevent accidental sample disruption or sensor tip breakage
24	Reference values take more time than usual to return to original baseline	Disturbed medium and/or dirty sensor tip with attached debris from the sample	Allow stabilization (~1 min) of the medium. Gently pipette the medium at the sensor tip to remove debris from the fluorophore; allow re-stabilization. After the experiment, rinse with dH_2O and wash with liquid soap if required. Often, however, even a dirty tip yields reliable data, because of the robust fluorescence quenching-based sensing mechanism
27	Micro-optrode does not retract	Salt crystallization or otherwise dirty housing needle blocks retraction	Do not force the plunger; it may lead to tip breaking. Immerse the needle in dH_2O for 5–10 min to dissolve and/or drain debris inside the needle

Timing

1. Steps 1–6, micro-optrode calibration: 30 min (one time per day of measurements) plus (one-time) 15 min to make the pO_2 0% solution
2. Steps 7–13, micro-optrode validation: 1.5 h (one time per micro-optrode) for the N_2 artificial sink
3. Step 14, data acquisition setup: 5 min for ASET software setup. Sampling rule optimization (Box 3) requires preliminary data acquisition to test the rules, thus the timing is dependent on the experimental design. It took us 1 h to optimize sampling rules using amputated tadpoles; however, that timing rose to 3 h because of the use of multiple biological replicates
4. Steps 15–27, experimental measurements: 30 min (one time) for the making of the dissecting and measurement chambers; 5–45 min for sample preparation, depending on specimen and conditions; measurement timing is dependent on the experimental design, e.g., for gill measurements (single ROI), 7 min per tadpole; and for a wounded cornea profile (multiple ROIs: wound edges, center and sides), 30 min per eye
5. Steps 28 and 29, data analysis: 1–2 h (one time) for template Excel worksheet (preconfiguration and formatting of multiple sheets with instructions, formulas and plots); <10 s per raw data file for extraction of data into the worksheet (copy and paste); 1 min per raw data file for flux calculation and visualization; 1–5 min for ROI selection, outlier removal (e.g., noise before signal stabilization, transient spikes) and mean calculation, according to the number of ROIs and trace noise; and 5–10 min for statistical analysis

Anticipated results

For a holistic overview of the micro-optrode capabilities and potentialities in animal physiology, we followed a multi-level analysis (from the cellular to the appendage level) in disparate animal models (from lower to higher vertebrates) and recorded various physiological responses.

A de novo mounted turnkey SMOT system (Fig. 1) should be validated. Full micro-optrode operationally is a proxy validation of the entire setup (Fig. 2). Using an artificial sink (N_2 (gas) bubble at capillary tip), a natural sink (tadpole gills) and a natural source (H_2O_2-iduced O_2 efflux in oocytes), we validated the micro-optrode per O_2 flux direction and magnitude of efficient detection. The O_2 influx decreases as the micro-optrode moves away from the sink (Fig. 2d–f), showing a significant exponential drop of flux with distance (r^2 = 0.99 or 0.98 in an artificial or natural sink, respectively; Fig. 2e–g). O_2 flux reversion was successfully recorded by the micro-optrode (Fig. 2h). We also tested the sensor against inert glass beads, showing it to be artifact free (Fig. 2i). In addition to the single micro-optrode mode, we also successfully validated the dual micro-optrode

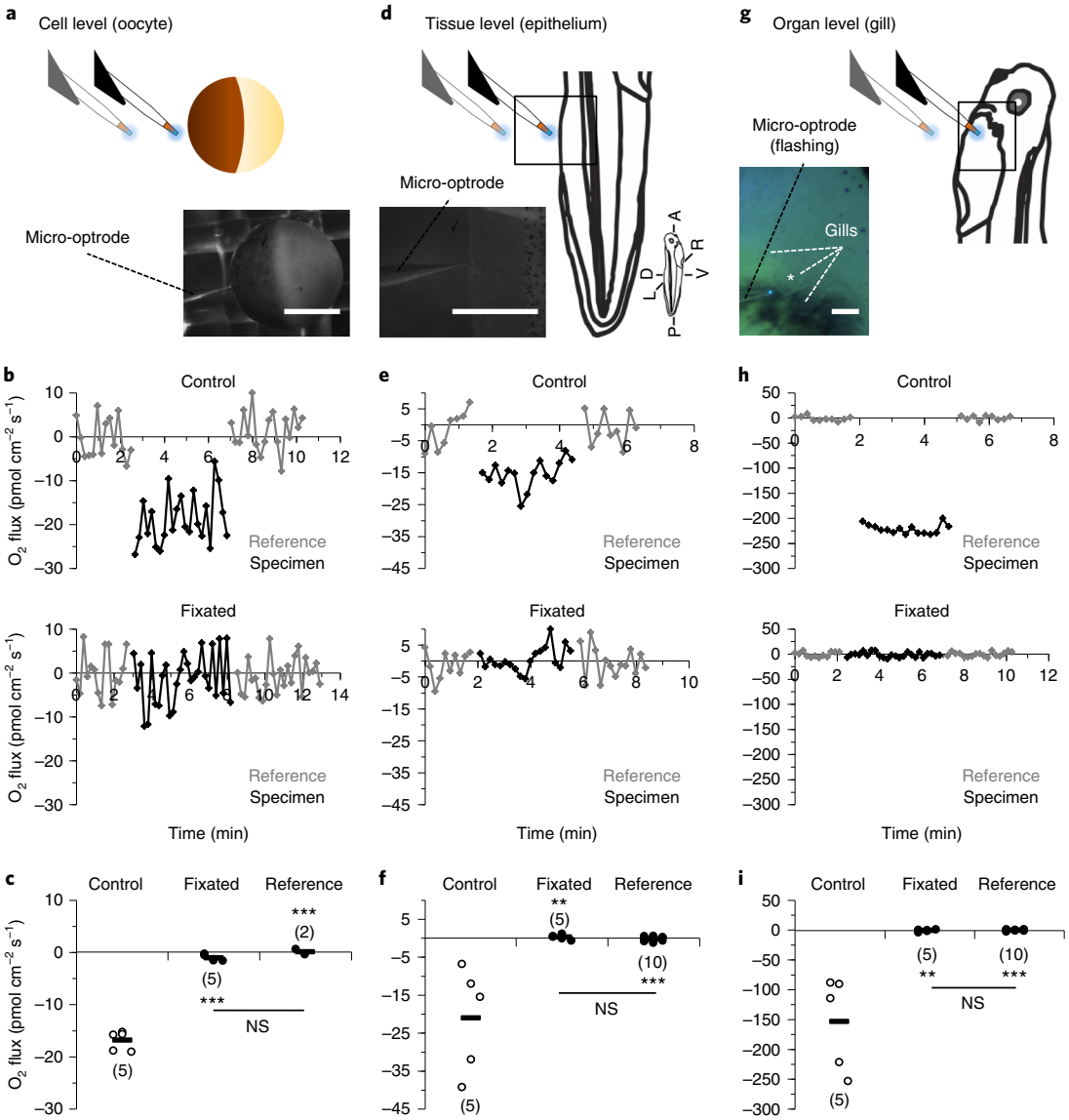

Fig. 4 | Multi-level oxygen flux as a marker for physiological status and viability. a–i, Measurement of endogenous oxygen fluxes in control and fixated (4% (wt/vol) PFA overnight) *X. laevis* oocytes (cell level) (**a**–**c**), tadpole epithelium (tissue level) (**d**–**f**) and tadpole gill (organ level) (**g**–**i**). **a**,**d**, **g**, Experimental design. Measurements were acquired in 1× (oocytes) or 0.1× (tadpoles) MMR. Gill measurements were from the middle gill of left axis (white *). Tadpole drawing (lateral view) is displayed in the same orientation as the whole organism anteroposterior (A–P), dorsoventral (D–V) and left–right (L–R) axes (bottom right scheme). Scale bars, ~0.5 mm (**a**, **d**); ~100 µm (**g**). **b**,**e**,**h**, Representative results. Top plots, control; bottom plots, fixated. *y* axis labels in **b** also apply to **e** and **h**. *x* axis labels in bottom plots also apply to top plots. **c**,**f**,**i**, Distributions and statistics. *y* axis label in **c** also applies to **f** and **i**. Data are presented using dot plots with mean lines. Statistical comparisons were performed using the unpaired Student's *t* test (two-tailed *P* value). NS, non-significant; $^{**}P < 0.01$; $^{***}P < 0.001$; number of biological replicates indicated in parentheses. All procedures involving animals were approved by the relevant institutional and national regulatory boards. Drawings (tadpoles), Erin Dewalt/Springer Nature.

mode, following the same reasoning (Fig. 3a–c). Using both modes in the same N_2 (gas) bubble, the resulting correlations of flux and distance were similar ($r^2 = 0.89$ or 0.90 in dual or single mode, respectively; Fig. 3d).

After validating the technique, we started to apply the micro-optrode (in single mode) as a way to verify the physiological integrity and viability of specimens (Fig. 4). To achieve this, we performed PFA-based fixation of specimens and measured O_2 fluxes at the cell (oocytes; Fig. 4a,b), tissue (tadpole epithelium; Fig. 4d,e) and organ (tadpole gill; Fig. 4g,h) levels. Compared to fluxes in viable specimens, fixation eliminated the fluxes ($P < 0.01$), which became identical to the reference baseline ($P > 0.05$; Fig. 4c,f,i). These assays also work as negative controls, attesting the proper response of the micro-optrode.

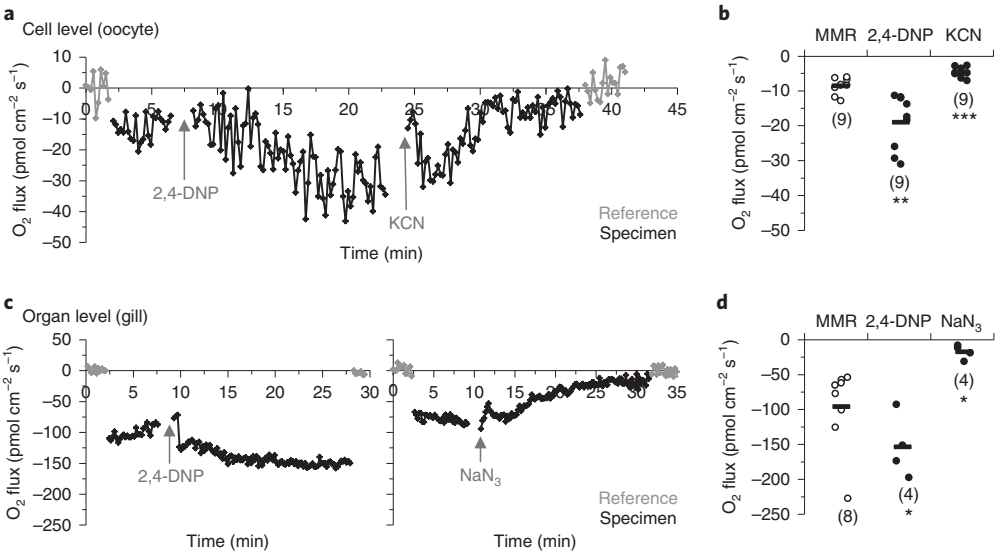

Fig. 5 | Multi-level oxygen flux in animal respiration. a–d, Measurement of endogenous oxygen fluxes in *X. laevis* oocytes (cell level; **a**,**b**) and tadpole gills (organ level; **c**,**d**) with and without respiratory electron chain transport drug blocker (1 mM KCN (**a**,**b**) or 2 mM NaN_3 (**c**,**d**)) and stimulator (100 µM (oocytes) or 50 µM (gills) 2,4-DNP). Experimental design as in Fig. 4. **a**,**c**, Representative results. Drug inoculation times annotated. **b**,**d**, Distributions (of peak plateaus for drug treatment) and statistics. Inoculation of the vehicle-control for 2,4-DNP (DMSO) had non-significant effect in O_2 flux. Data are presented using dot plots with mean lines. Statistical comparisons were performed using the unpaired Student's *t* test (two-tailed *P* value for oocytes and one-tailed *P* value for tadpole siblings). $*P < 0.05$; $**P < 0.01$; $***P < 0.001$; number of biological replicates indicated in parentheses. All procedures involving animals were approved by the relevant institutional and national regulatory boards.

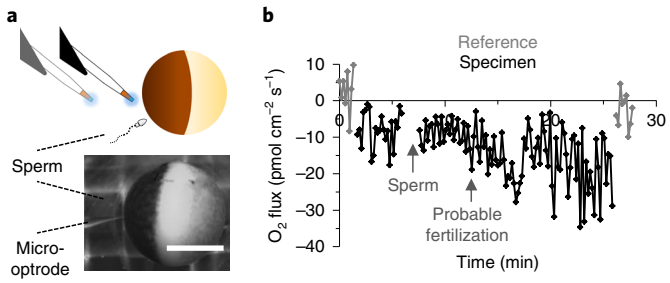

Fig. 6 | Oxygen flux in animal in vitro fertilization (IVF). a, Experimental design; ~20% of a testis preserved at 4 °C was macerated in water. 100 µl of this sperm solution was inoculated into the measuring chamber. Scale bar, 0.5 mm. **b**, Measurement of endogenous oxygen flux before and after sperm inoculation (annotated). Fertilization induces an increase and peak of O_2 consumption. All procedures involving animals were approved by the relevant institutional and national regulatory boards.

Next, we studied obvious physiological candidates: respiration and bioenergetics. We used drugs modulating the cellular respiration in oocytes (cell level; Fig. 5a,b) and tadpole gills (organ level; Fig. 5c,d). The use of a stimulator of the respiratory electron chain transport (2,4-DNP) showed more than double the O_2 influx magnitude in both specimens ($P < 0.05$; Fig. 5b,d). Congruently, the use of an electron chain transport blocker (KCN or NaN_3) significantly abrogated O_2 influx ($P < 0.05$; Fig. 5b,d). These results are also important negative and positive experimental controls that guarantee the acqusition of robust experimental measurements.

Then we applied the micro-optrode to observe the characteristic increase in O_2 uptake upon fertilization (Fig. 6)[72]. For this, during continual recording, we inoculated the sperm solution (from macerated testis) into the chamber with an oocyte (Fig. 6a). A peak and increased O_2 influx occurred at the probable moment of fertilization (Fig. 6b).

Finally, we show comprehensive results of the O_2 dynamics in wound healing and regeneration (Fig. 7), extracted mainly from the original data recently published[24]. We created wounds from the

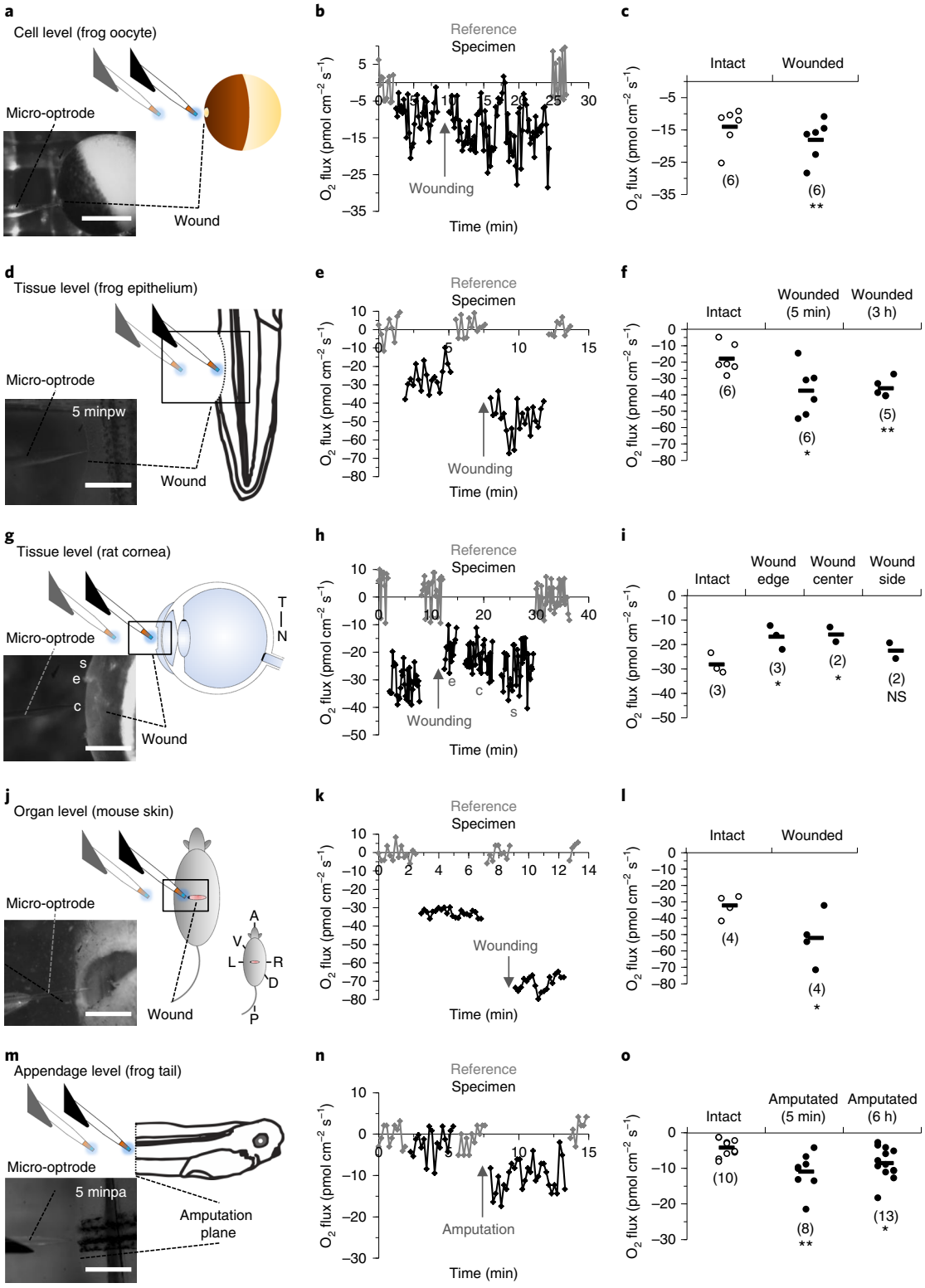

cellular to the organ level, respectively, in oocytes (Fig. 7a) and tadpole epithelium (Fig. 7d), rat cornea (Fig. 7g) and non-diabetic mouse skin (Fig. 7j), and measured the effect on O_2 influx magnitude. Also, we amputated half of tadpole tails (appendage level; Fig. 7m) to demonstrate a concomitant shift in O_2 fluxes. Interestingly, wounding or amputation resulted in a sustained increased of O_2 influx at the cell ($P < 0.001$; Fig. 7b,c), tissue ($P < 0.05$; Fig. 7e,f), organ ($P < 0.05$; Fig. 7k,l) and

◀ **Fig. 7 | Multi-level oxygen flux in wound healing and regeneration. a–o**, Measurement of endogenous oxygen fluxes in intact and wounded or amputated *X. laevis* oocytes (cell level) (**a–c**), tadpole epithelium (tissue level) (**d–f**), rat corneal epithelium (tissue level) (**g–i**), non-diabetic mouse skin (organ level) (**j–l**) and tadpole tail (appendage level) (**m–o**). **a**,**d**,**g**,**j**,**m**, Experimental design. Measurements were acquired in MMR 1× (oocytes) or 0.1× (tadpoles), artificial tear solution (BSS+; rat cornea) or PBS (1×; mouse skin). For the measurements, we used isolated whole eyes enucleated from euthanized 7–8-week-old male Sprague–Dawley rats and euthanized 8-week-old male BKS.Cg-*Dock7*^{m} +/+ *Lepr*^{db}/J heterozygous (non-diabetic) mice. Eye photomicrograph and scheme (lateral view) are displayed in the temporal (T) to nasal (N) axis orientation. minpw, minutes post-wounding; minpa, minutes post-amputation. c, center; e, edge; s, side. Mouse photomicrograph and scheme (top view) are displayed in the same orientation as the whole organism anteroposterior (A–P), dorsoventral (D–V) and left–right (L–R) axes (bottom right scheme). Scale bars, ~0.5 mm (**a**,**d**); ~1 mm (**g**,**j**,**m**). **b**,**e**,**h**,**k**,**n**, Representative results. Wounding and amputation times annotated. **c**,**f**,**i**,**l**,**o**, Distributions and statistics. Data of **c**, **f**, **l** and **o** were originally published in ref. [24]; complete spatiotemporal profiling of **f** and **o** can be found in the same study. Data are presented using dot plots with mean lines. Statistical comparisons were performed using the paired Student's *t* test (two-tailed *P* value for oocytes and one-tailed *P* value for mice) and unpaired Student's *t* test (two-tailed *P* value for tadpoles and one-tailed *P* value for rat). NS, non-significant; $*P < 0.05$; $**P < 0.01$; number of biological replicates indicated in parentheses. All procedures involving animals were approved by the relevant institutional and national regulatory boards. Drawings (tadpoles), Erin Dewalt/Springer Nature.

Box 5 | Oscillatory behavior

Oxygen is a major player in metabolic and signaling pathways; therefore, it might display or be subjected to oscillatory behavior[73–75]. Intriguingly, we noticed that in many recordings, the O_2 flux appears to stabilize in an oscillatory manner rather than in a flat plateau. Oscillations with a frequency (*f*) range of 4–8 mHz (2–4 min period (*T*; peak-to-peak time)) were not uncommon (see figure, representative result of a wounded tadpole epithelium). Owing to our research goals, we usually acquired data in the same sampling locus (ROI) for 2–5 min. Thus, we could not robustly study oscillations and definitively identify false-positive and false-negative readouts[24]. However, with an increase in recording time, this technique is perfectly suitable to the study of oscillations.

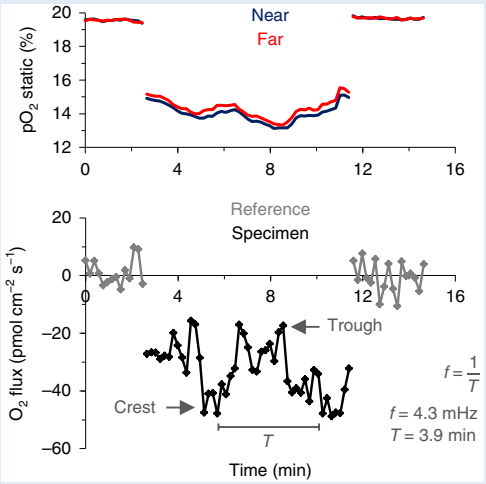

appendage ($P < 0.05$; Fig. 7n, o) levels. The exception was in the corneal wounding, in which influx decreased instead ($P < 0.05$; Fig. 7h,i). We showed that the elevated influx is caused by barrier breaking and its purpose is to fuel ROS production, important for healing and regeneration[24]. In the case of rat cornea, the lower magnitude is probably due to the virtual absence of epithelial cells (scraped off until stroma); we are following up this line of research in a new study.

Intriguingly, many recordings, in the different animal models used, appear to present oscillations in the O_2 fluxes (Box 5). The oscillatory behavior may be the result or an epiphenomenon of the key role of O_2 in bioenergetics and metabolism (e.g., mitochondrial activity) and in signaling pathways (e.g., Ca^{2+})[47,73–75]. Future studies using this technique that are directed at researching O_2 flux oscillations may uncover fundamental aspects of cell and oxic biology. Furthermore, the technique may become part of the life sciences toolkit to assist researchers in their findings. In conclusion, we

described a powerful research tool—optics-based measurement of oxygen dynamics—with high sensitivity, and temporal and spatial resolution, which investigators can use without excessive expenditure and training.

Reporting Summary

Further information on research design is available in the Nature Research Reporting Summary linked to this article.

Data availability

The representative data that support and use the approach are included in this protocol. Extended data are available in the support research paper[24]. In addition, all primary data underlying the figures shown in this protocol are available from the corresponding authors upon reasonable request.

References

1. Holland, H. D. The oxygenation of the atmosphere and oceans. *Philos. Trans. R. Soc. Lond. B Biol. Sci.* **361**, 903–915 (2006).
2. Semenza, G. L. Life with oxygen. *Science* **318**, 62–64 (2007).
3. Lane, N. & Martin, W. The energetics of genome complexity. *Nature* **467**, 929–934 (2010).
4. Graham, J. B., Dudley, R., Aguilar, N. M. & Gans, C. Implications of the late palaeozoic oxygen pulse for physiology and evolution. *Nature* **375**, 117–120 (1995).
5. Cloud, P. E. Atmospheric and hydrospheric evolution on the primitive Earth. *Science* **160**, 729–736 (1968).
6. Simon, M. C. & Keith, B. The role of oxygen availability in embryonic development and stem cell function. *Nat. Rev. Mol. Cell Biol.* **9**, 285–296 (2008).
7. Brahimi-Horn, M. C. & Pouysségur, J. Oxygen, a source of life and stress. *FEBS Lett.* **581**, 3582–3591 (2007).
8. Jarecki, J., Johnson, E. & Krasnow, M. A. Oxygen regulation of airway branching in Drosophila is mediated by branchless FGF. *Cell* **99**, 211–220 (1999).
9. Compernolle, V. et al. Loss of HIF-2alpha and inhibition of VEGF impair fetal lung maturation, whereas treatment with VEGF prevents fatal respiratory distress in premature mice. *Nat. Med.* **8**, 702–710 (2002).
10. Shweiki, D., Itin, A., Soffer, D. & Keshet, E. Vascular endothelial growth factor induced by hypoxia may mediate hypoxia-initiated angiogenesis. *Nature* **359**, 843–845 (1992).
11. Genbacev, O., Zhou, Y., Ludlow, J. W. & Fisher, S. J. Regulation of human placental development by oxygen tension. *Science* **277**, 1669–1672 (1997).
12. Morriss, G. M. & New, Da. T. Effect of oxygen concentration on morphogenesis of cranial neural folds and neural crest in cultured rat embryos. *J. Embryol. Exp. Morphol.* **54**, 17–35 (1979).
13. Gustafsson, M. V. et al. Hypoxia requires Notch signaling to maintain the undifferentiated cell state. *Dev. Cell* **9**, 617–628 (2005).
14. Gilkes, D. M., Semenza, G. L. & Wirtz, D. Hypoxia and the extracellular matrix: drivers of tumour metastasis. *Nat. Rev. Cancer* **14**, 430–439 (2014).
15. Ryan, H. E., Lo, J. & Johnson, R. S. HIF-1α is required for solid tumor formation and embryonic vascularization. *EMBO J.* **17**, 3005–3015 (1998).
16. Covello, K. L. et al. HIF-2alpha regulates Oct-4: effects of hypoxia on stem cell function, embryonic development, and tumor growth. *Genes Dev.* **20**, 557–570 (2006).
17. Guo, X. et al. The galvanotactic migration of keratinocytes is enhanced by hypoxic preconditioning. *Sci. Rep.* **5**, 1–13 (2015).
18. Niethammer, P., Grabher, C., Look, A. T. & Mitchison, T. J. A tissue-scale gradient of hydrogen peroxide mediates rapid wound detection in zebrafish. *Nature* **459**, 996–999 (2009).
19. Sen, C. K. & Roy, S. Redox signals in wound healing. *Biochim. Biophys. Acta* **1780**, 1348–1361 (2008).
20. Sunkari, V. G. et al. Hyperbaric oxygen therapy activates hypoxia-inducible factor 1 (HIF-1), which contributes to improved wound healing in diabetic mice. *Wound Repair Regen.* **23**, 98–103 (2015).
21. Ferreira, F., Luxardi, G., Reid, B. & Zhao, M. Early bioelectric activities mediate redox-modulated regeneration. *Development* **143**, 4582–4594 (2016).
22. Love, N. R. et al. Amputation-induced reactive oxygen species are required for successful Xenopus tadpole tail regeneration. *Nat. Cell Biol.* **15**, 222–228 (2013).
23. Zhang, Y. et al. Drug-induced regeneration in adult mice. *Sci. Transl. Med.* **7**, 1–11 (2015).
24. Ferreira, F., Raghunathan, V., Luxardi, G., Zhu, K. & Zhao, M. Early redox activities modulate Xenopus tail regeneration. *Nat. Commun.* **9**, 1–15 (2018).
25. Lambeth, J. D. & Neish, A. S. Nox enzymes and new thinking on reactive oxygen: a double-edged sword revisited. *Annu. Rev. Pathol.* **9**, 119–145 (2014).
26. Auten, R. L. & Davis, J. M. Oxygen toxicity and reactive oxygen species: the devil is in the details. *Pediatr. Res.* **66**, 121–127 (2009).
27. Semenza, G. L. Regulation of mammalian oxygen homeostasis by hypoxia-inducible factor 1. *Annu. Rev. Cell Dev. Biol.* **15**, 551–578 (1999).

28. Chaturvedi, P. et al. Emerging technologies for non-invasive quantification of physiological oxygen transport in plants. *Planta* **238**, 599–614 (2013).
29. Stern, O. & Volmer, M. über die Abklingzeit der Fluoreszenz. *Z. Phys.* **20**, 183–188 (1919).
30. Kautsky, H. Quenching of luminescence by oxygen. *Trans. Faraday Soc.* **35**, 216–219 (1939).
31. Lakowicz, J. R. Quenching of fluorescence. in *Principles of Fluorescence Spectroscopy* 277–330 (Springer, US, 2006).
32. Wang, X. & Wolfbeis, O. S. Optical methods for sensing and imaging oxygen: materials, spectroscopies and applications. *Chem. Soc. Rev.* **43**, 3666–3761 (2014).
33. Kautsky, H. & Hirsch, A. Interactions of excited dye molecules and oxygen. *Ber. Dtsch. Chem. Ges.* **64**, 2677–2686 (1931).
34. Lübbers, D. W. & Opitz, N. The pCO2/pO2-optode: a new probe for measurement of pCO2 or pO2 in fluids and gases. *Z. Naturforsch. C. J. Biosci.* **30**, 532–533 (1975).
35. Wolfbeis, O. S. & Weidgans, B. M. Fiber optic chemical sensors and biosensors: a view back. in *Optical Chemical Sensors. NATO Science Series II: Mathematics, Physics and Chemistry* (eds. Baldini, F., Chester, A., Homola, J. & Martellucci, S.) 17–44 (Springer, Dordrecht, 2006).
36. Peterson, J. I., Fitzgerald, R. V. & Buckhold, D. K. Fiber-optic probe for in vivo measurement of oxygen partial pressure. *Anal. Chem.* **56**, 62–67 (1984).
37. Lippitsch, M. E., Pusterhofer, J., Leiner, M. J. P. & Wolfbeis, O. S. Fibre-optic oxygen sensor with the fluorescence decay time as the information carrier. *Anal. Chim. Acta* **205**, 1–6 (1988).
38. Klimant, I., Meyer, V. & Kühl, M. Fiber-optic oxygen microsensors, a new tool in aquatic biology. *Limnol. Oceanogr.* **40**, 1159–1165 (1995).
39. Klimant, I., Ktil, M., Glud, R. N. & Holst, G. Optical measurement of oxygen and temperature in microscale: strategies and biological applications. *Sens. Actuators B Chem.* **39**, 29–37 (1997).
40. Krihak, M. K. & Shahriari, M. R. Highly sensitive, all solid state fibre optic oxygen sensor based on the sol-gel coating technique. *Electron. Lett.* **32**, 240–242 (1996).
41. Kühl, M. & Jørgensen, B. B. Spectral light measurements in microbenthic phototrophic communities with a fiber-optic microprobe coupled to a sensitive diode array detector. *Limonol. Oceanogr.* **37**, 1813–1823 (1992).
42. Lee, S.-K. & Okura, I. Photostable optical oxygen sensing material: platinum tetrakis(pentafluorophenyl) porphyrin immobilized in polystyrene. *Anal. Commun.* **34**, 185–188 (1997).
43. Porterfield, D. M., Rickus, J. L. & Kopelman, R. Noninvasive approaches to measuring respiratory patterns using a PtTFPP based phase-lifetime self-referencing oxygen optrode. *Proc. SPIE* **6380**, 63800S (SPIE, 2006).
44. Wolfbeis, O. S. Optical technology until the year 2000: an historical overview. in *Optical Sensors. Springer Series on Chemical Sensors andBiosensors (Methods and Applications)*, Vol. 1 1–34 (Springer, Berlin Heidelberg, 2004).
45. Chatni, M. R., Li, G. & Porterfield, D. M. Frequency-domain fluorescence lifetime optrode system design and instrumentation without a concurrent reference light-emitting diode. *Appl. Opt.* **48**, 5528–5536 (2009).
46. Xin, X. et al. A real-time, non-invasive, micro-optrode technique for detecting seed viability by using oxygen influx. *Sci. Rep.* **3**, 3057 (2013).
47. McLamore, E. S., Jaroch, D., Chatni, M. R. & Porterfield, D. M. Self-referencing optrodes for measuring spatially resolved, real-time metabolic oxygen flux in plant systems. *Planta* **232**, 1087–1099 (2010).
48. Wan, Y. *et al.* Non-invasive measurement of real-time oxygen flux in plant systems with a self-referencing optrode. *Protoc. Exch.* (2011). https://doi.org/10.1038/protex.2011.266
49. Chatni, M. R. & Porterfield, D. M. Self-referencing optrode technology for non-invasive real-time measurement of biophysical flux and physiological sensing. *Analyst* **134**, 2224–2232 (2009).
50. Plitzko, B. & Loesgen, S. Measurement of oxygen consumption rate (OCR) and extracellular acidification rate (ECAR) in culture cells for assessment of the energy metabolism. *Bio-Protoc.* **8**, e2850 (2018).
51. Wolfbeis, O. S. Luminescent sensing and imaging of oxygen: fierce competition to the Clark electrode. *BioEssays* **37**, 921–928 (2015).
52. Clark, L. C. J., Wolf, R., Granger, D. & Taylor, Z. Continuous recording of blood oxygen tensions by polarography. *J. Appl. Physiol.* **6**, 189–193 (1953).
53. Ingram, J. M., Zhang, C., Xu, J. & Schiff, S. J. FRET excited ratiometric oxygen sensing in living tissue. *J. Neurosci. Methods* **214**, 45–51 (2013).
54. Jorge, P. A. S. et al. Applications of quantum dots in optical fiber luminescent oxygen sensors. *Appl. Opt.* **45**, 3760–3767 (2006).
55. Düssmann, H., Perez-Alvarez, S., Anilkumar, U., Papkovsky, D. B. & Prehn, J. H. Single-cell time-lapse imaging of intracellular O2 in response to metabolic inhibition and mitochondrial cytochrome-c release. *Cell Death Dis.* **8**, e2853 (2017).
56. Land, S. C., Porterfield, D. M., Sanger, R. H. & Smith, P. J. The self-referencing oxygen-selective microelectrode: detection of transmembrane oxygen flux from single cells. *J. Exp. Biol.* **202**, 211–218 (1999).
57. Lamboursain, L., St-Onge, F. & Jolicoeur, M. A lab-built respirometer for plant and animal cell culture. *Biotechnol. Prog.* **18**, 1377–1386 (2002).
58. Severinghaus, J. W. The invention and development of blood gas analysis. *Anesthesiology* **97**, 253–256 (2002).
59. Xiong, L. & Compton, R. G. Amperometric gas detection: a review. *Int. J. Electrochem. Sci.* **9**, 7152–7181 (2014).
60. Kühtreiber, W. M. & Jaffe, L. F. Detection of extracellular calcium gradients with a calcium-specific vibrating electrode digital version can attain a noise level of less than. *J. Cell Biol.* **110**, 1565–1573 (1990).

61. Jaffe, L. F. & Nuccitelli, R. An ultrasensitive vibrating probe for measuring steady extracellular currents. *J. Cell Biol.* **63**, 614–628 (1974).
62. Kunkel, J. G., Cordeiro, S., Xu, Y. J., Shipley, A. M. & José, A. The use of non-invasive ion-selective microelectrode techniques for the study of plant development. in *Plant Electrophysiology: Theory and Methods* (ed., Volkov, A.G.) 109–137 (Springer, 2006).
63. Zisman, W. A. A new method of measuring contact potential differences in metals. *Rev. Sci. Instrum.* **3**, 367–370 (1932).
64. Porterfield, D. M. Measuring metabolism and biophysical flux in the tissue, cellular and sub-cellular domains: recent developments in self-referencing amperometry for physiological sensing. *Biosens. Bioelectron.* **22**, 1186–1196 (2007).
65. Taryba, M. G., Montemor, M. F. & Lamaka, S. V. Quasi-simultaneous mapping of local current density, pH and dissolved O_2. *Electroanalysis* **27**, 2725–2730 (2015).
66. Chu, C.-S. & Su, C.-J. Optical fiber sensor for dual sensing of H2O2 and DO based on CdSe/ZnS QDs and Ru (dpp)32+ embedded in EC matrix. *Sens. Actuators B Chem.* **255**, 1079–1086 (2018).
67. Jamnongwong, M., Loubiere, K., Dietrich, N. & Hébrard, G. Experimental study of oxygen diffusion coefficients in clean water containing salt, glucose or surfactant: consequences on the liquid-side mass transfer coefficients. *Chem. Eng. J.* **165**, 758–768 (2010).
68. Luxardi, G., Reid, B., Ferreira, F., Maillard, P. & Zhao, M. Measurement of extracellular ion fluxes using the ion-selective self-referencing microelectrode technique. *J. Vis. Exp.* **2015**, e52782 (2015).
69. Shen, Y. et al. Diabetic cornea wounds produce significantly weaker electric signals that may contribute to impaired healing. *Sci. Rep.* **6**, 1–11 (2016).
70. Reid, B., Nuccitelli, R. & Zhao, M. Non-invasive measurement of bioelectric currents with a vibrating probe. *Nat. Protoc.* **2**, 661–669 (2007).
71. Han, P. & Bartels, D. M. Temperature dependence of oxygen diffusion in H_2O and D_2O. *J. Phys. Chem.* **100**, 5597–5602 (1996).
72. Lopes, A. S., Lane, M. & Thompson, J. G. Oxygen consumption and ROS production are increased at the time of fertilization and cell cleavage in bovine zygotes. *Hum. Reprod.* **25**, 2762–2773 (2010).
73. Stringari, C. et al. In vivo single-cell detection of metabolic oscillations in stem cells. *Cell Rep.* **10**, 1–7 (2015).
74. Cai, H. et al. Nucleocytoplasmic shuttling of a GATA transcription factor functions as a development timer. *Science* **343**, 1249531 (2014).
75. Feijó, J. A. et al. Cellular oscillations and the regulation of growth: the pollen tube paradigm. *BioEssays* **23**, 86–94 (2001).
76. Lakowicz, J. R. Frequency-domain lifetime measurements. in *Principles of Fluorescence Spectroscopy* 157–204 (Springer, US, 2006).
77. Demas, J. N., DeGraff, B. A. & Xu, W. Modeling of Luminescence Quenching-Based Sensors: Comparison of Multisite and Nonlinear Gas Solubility Models. *Anal. Chem.* **67**, 1377–1380 (2005).
78. Lide, D. R. *CRC Handbook of Chemistry and Physics* (CRC Press, 2005).

Acknowledgements

This work was supported by two NIH grants (EY019101 and R21EB015737), an AFOSR grant (FA9550-16-1-0052) and by an unrestricted grant from Research to Prevent Blindness, Inc., to the University of California (UC), Davis Ophthalmology Department. F.F. was supported by Fundação para a Ciência e Tecnologia (FCT) grant SFRH/BD/87256/2012. We thank A. Gomes (Departamento de Biologia, CBMA, Universidade do Minho, Portugal) for support. We are grateful to A. L. Miller (Department of Biology, Hong Kong University of Science and Technology, China), M. Horb (director of the NXR, MBL) and E. Pearl (NXR, MBL), as well as A. M. Shipley (Applicable Electronics) for generously hosting F.F.'s visit to MBL (summer 2014), for help in providing access to local research facilities and materials (SMOT and tadpoles (NXR RRID: SCR_013731) included), and for helpful comments. We are also grateful to C. A. Shipley, Applicable Electronics, for lending a SMOT system to the Zhao lab. We offer special thanks to E. Karplus (Science Wares, Inc.), designer and programmer of the SMOT, for providing software, technical assistance and support for its efficient installation and operation. We appreciate the input given by A. M. Shipley and E. Karplus to establish an efficient protocol in the Zhao lab. We are further thankful to E. Karplus for helping with the mathematics and interpretation behind the equations used to calculate O_2 flux. We are grateful to Y. Yu (Department of Molecular & Cell Biology, UC Berkeley) for generously providing glass beads and for helpful discussion. We appreciate the technical information about micro-optrodes provided by S. Kerschensteiner and C. Huber (PreSens, GmbH). We thank Y. Shen (Department of Dermatology, UC Davis; Department of Occupational and Environmental Health, Zhejiang University, China) for kindly providing the euthanized mice. We thank the Zhao lab members for helpful discussions.

Author contributions

F.F. designed and optimized the protocol. G.L. provided training in oocyte wounding. B.R. provided the intact and wounded rat eyes. L.M. executed some experiments. F.F. performed the physiological measurements and analyzed the data. M.Z. provided the funds for experiments and manuscript. All authors contributed to the scientific discussions and study design as appropriate. F.F. wrote the manuscript. B.R., VK.R. and M.Z. edited the manuscript. All authors read, commented and accepted the final manuscript.

Competing interests

F.F. and M.Z. declare the existence of a non-financial competing interest. The measurements were performed using turnkey systems provided free for use at MBL and lent to the Zhao lab at no cost by Applicable Electronics, LLC, and Science Wares, Inc. The companies had no influence over the research (design, execution or interpretation), or its reporting; no restrictions on data sharing have been imposed. The other authors declare no competing interests.

Additional information

Supplementary information is available for this paper at https://doi.org/10.1038/s41596-019-0231-x.

Reprints and permissions information is available at www.nature.com/reprints.

Correspondence and requests for materials should be addressed to F.F. or M.Z.

Peer review information *Nature Protocols* thanks D. Marshall Porterfield, Otto S. Wolfbeis and other anonymous reviewer(s) for their contribution to the peer review of this work.

Publisher's note Springer Nature remains neutral with regard to jurisdictional claims in published maps and institutional affiliations.

Received: 30 October 2018; Accepted: 31 July 2019;
Published online: 10 January 2020

Related link

Key reference using this protocol

Ferreira, F., Raghunathan, V., Luxardi, G., Zhu, K. & Zhao, M. *Nat. Commun.* **9**, 4296 (2018): https://www.nature.com/articles/s41467-018-06614-2

nature research

Corresponding author(s): Fernando Ferreira, Min Zhao

Reporting Summary

Nature Research wishes to improve the reproducibility of the work that we publish. This form provides structure for consistency and transparency in reporting. For further information on Nature Research policies, see Authors & Referees and the Editorial Policy Checklist.

Statistical parameters

When statistical analyses are reported, confirm that the following items are present in the relevant location (e.g. figure legend, table legend, main text, or Methods section).

n/a	Confirmed	
☐	☒	The exact sample size (*n*) for each experimental group/condition, given as a discrete number and unit of measurement
☐	☒	An indication of whether measurements were taken from distinct samples or whether the same sample was measured repeatedly
☐	☒	The statistical test(s) used AND whether they are one- or two-sided *Only common tests should be described solely by name; describe more complex techniques in the Methods section.*
☐	☒	A description of all covariates tested
☐	☒	A description of any assumptions or corrections, such as tests of normality and adjustment for multiple comparisons
☐	☒	A full description of the statistics including central tendency (e.g. means) or other basic estimates (e.g. regression coefficient) AND variation (e.g. standard deviation) or associated estimates of uncertainty (e.g. confidence intervals)
☐	☒	For null hypothesis testing, the test statistic (e.g. *F*, *t*, *r*) with confidence intervals, effect sizes, degrees of freedom and *P* value noted *Give P values as exact values whenever suitable.*
☒	☐	For Bayesian analysis, information on the choice of priors and Markov chain Monte Carlo settings
☒	☐	For hierarchical and complex designs, identification of the appropriate level for tests and full reporting of outcomes
☒	☐	Estimates of effect sizes (e.g. Cohen's *d*, Pearson's *r*), indicating how they were calculated
☐	☒	Clearly defined error bars *State explicitly what error bars represent (e.g. SD, SE, CI)*

Our web collection on statistics for biologists may be useful.

Software and code

Policy information about availability of computer code

Data collection	No custom software was used.
Data analysis	No custom software was used.

For manuscripts utilizing custom algorithms or software that are central to the research but not yet described in published literature, software must be made available to editors/reviewers upon request. We strongly encourage code deposition in a community repository (e.g. GitHub). See the Nature Research guidelines for submitting code & software for further information.

Data

Policy information about availability of data

All manuscripts must include a data availability statement. This statement should provide the following information, where applicable:

- Accession codes, unique identifiers, or web links for publicly available datasets
- A list of figures that have associated raw data
- A description of any restrictions on data availability

The data (structured and representative) that support and use the protocol are embedded in the technical paper. Extended data are available in the support research paper (Ferreira et al., Nat. Comm. 9, 1–15 (2018)). In addition, other relevant data (discrete and numerical) are available unrestricted from the corresponding authors upon reasonable request.

Field-specific reporting

Please select the best fit for your research. If you are not sure, read the appropriate sections before making your selection.

☒ Life sciences ☐ Behavioural & social sciences ☐ Ecological, evolutionary & environmental sciences

For a reference copy of the document with all sections, see nature.com/authors/policies/ReportingSummary-flat.pdf

Life sciences study design

All studies must disclose on these points even when the disclosure is negative.

Sample size	No sample size calculation. Observed differences were generally very large, so around 5 specimens randomly collected from different batches were typically deemed sufficient and used.
Data exclusions	Pre-established exclusion criteria: exclude data if control siblings readout is too inconsistent with average across independent experiments. Majority of data points were accepted, in fact, outliers are shown in boxplots.
Replication	Replication was successful.
Randomization	Randomization was achieved by randomly collecting live samples from large batches.
Blinding	Blinding was deemed unnecessary.

Reporting for specific materials, systems and methods

Materials & experimental systems

n/a	Involved in the study
☒	☐ Unique biological materials
☒	☐ Antibodies
☒	☐ Eukaryotic cell lines
☒	☐ Palaeontology
☐	☒ Animals and other organisms
☒	☐ Human research participants

Methods

n/a	Involved in the study
☒	☐ ChIP-seq
☒	☐ Flow cytometry
☒	☐ MRI-based neuroimaging

Animals and other organisms

Policy information about studies involving animals; ARRIVE guidelines recommended for reporting animal research

Laboratory animals	Xenopus laevis (oocytes and tadpoles), Mus musculus (male BKS.Cg-Dock7m +/+ Leprdb/J heterozygous (non-diabetic) mice), Rattus norvegicus (male Sprague-Dawley rats).
Wild animals	Study did not involve wild animals.
Field-collected samples	Study did not involve samples collected from the field.